crystals

MDPI

Article

Crystal and Magnetic Structures in Layered, Transition Metal Dihalides and Trihalides

Michael A. McGuire

Materials Science and Technology Division, Oak Ridge National Laboratory, Oak Ridge, TN 37831, USA; mcguirema@ornl.gov

Academic Editor: Winnie Wong-Ng
Received: 20 March 2017 ; Accepted: 23 April 2017 ; Published: 27 April 2017

Abstract: Materials composed of two dimensional layers bonded to one another through weak van der Waals interactions often exhibit strongly anisotropic behaviors and can be cleaved into very thin specimens and sometimes into monolayer crystals. Interest in such materials is driven by the study of low dimensional physics and the design of functional heterostructures. Binary compounds with the compositions MX_2 and MX_3 where M is a metal cation and X is a halogen anion often form such structures. Magnetism can be incorporated by choosing a transition metal with a partially filled d-shell for M, enabling ferroic responses for enhanced functionality. Here a brief overview of binary transition metal dihalides and trihalides is given, summarizing their crystallographic properties and long-range-ordered magnetic structures, focusing on those materials with layered crystal structures and partially filled d-shells required for combining low dimensionality and cleavability with magnetism.

Keywords: layered materials; van der Waals; monolayer; transition metal compounds; halides; crystal structure; magnetism; magnetic structure

1. Introduction

Binary transition metal halides MX_y (M = metal cation, X = halogen anion) provide a rich family of materials in which low dimensional magnetism can be examined, and such studies were carried out through much of the last century [1]. The dihalides contain triangular nets of transition metal cations, and geometrical frustration is expected when the magnetic interactions are antiferromagnetic (AFM) [2–4]. Several of the MX_2 compounds form helimagnetic structures and display multiferroic behavior [5–8]. In the trihalides, on the other hand, the transition metal cations form honeycomb nets. This lattice is not frustrated for simple AFM nearest neighbor interactions, but in the case of $RuCl_3$ more complex magnetic interactions and spin-orbit coupling are expected to result in a spin-liquid ground state that is currently of much interest [9–13]. For many of the materials considered here, the in plane interactions are ferromagnetic (FM). Chromium trihalides were identified as some of the earliest ferromagnetic semiconductors, and CrX_3 compounds in general have received recent attention as candidate materials for the study of magnetic monolayers and for use in van der Waals heterostructures, in which their magnetism can be coupled to electronic and optical materials via proximity effects [14–21]. Developing cleavable ferroic materials, both magnetic and electric, is key to expanding the toolbox available for designing and creating custom, functional heterostructures and devices [22–24]. Although FM and ferroelectric materials play the most clear role in such applications, the development of spintronics employing antiferromagnetic materials may open the door to a much larger set of layered transition metal halides [25–27].

It is generally observed that binary halides often form low dimensional crystal structures, comprising either molecular units, one dimensional chains, or two dimensional layers. This holds true especially for the chlorides, bromides, and iodides, and can be attributed to the low ionic charge X^-

and relatively large ionic radii (1.8–2.2 Å) of these anions. This results in multiple large anions for each metal cation assuming oxidation states typical for transition metals. Thus the cations are usually found in six-fold coordination and are well separated into structural units that are joined to one another in the crystal by van der Waals bonding between halogen anions. Fluoride has a much smaller ionic radius (1.3 Å) and forms three dimensional crystal structures with the divalent and trivalent cations that are the focus of most of this work. Note that this simple ionic picture is not appropriate when metal-metal bonding is present, which is often the case in the early, heavy transition metals. Typically larger anion to cation ratios result in lower dimensional structures, but often polymorphs of different dimensionality occur for a single composition. For example, $TiCl_3$ forms with 1D chains of face sharing octahedra or 2D layers of edge sharing octahedra [28,29]. Dihalides (MX_2) and trihalides (MX_3) represent the majority of layered binary transition metal halides. There are, however, other examples, including Nb_3Cl_8 [30], in which interesting magnetic behavior has been noted recently [31,32].

Here, a brief review of MX_2 and MX_3 compounds with partially filled *d*-shells is presented, with a focus on crystal and magnetic structures. A general overview of the crystallographic properties and magnetic behavior including static magnetic order in these two families is given. This short survey is not meant to be exhaustive, but rather to give a general introduction to these materials and a broad overview of the trends observed in their crystallographic and magnetic properties, with references to the literature where more detailed discussion can be found.

2. Crystal Structures of Layered, Binary, Transition Metal Halides

2.1. MX_2 Compounds

Crystal structure information for MX_2 compounds with partially filled *d*-shells is collected in Table 1. Non-magnetic, layered dihalides of Zn, Cd, and Hg, with valence electronic configurations $3d^{10}$, $4d^{10}$, and $5d^{10}$, respectively, are also known [33–39], but these are not considered here. It can be seen that most of the compounds in Table 1 adopt either the trigonal CdI_2 structure type or the rhombohedral $CdCl_2$ structure type. These structures are shown in Figure 1. Both contain triangular nets of cations in edge sharing octahedral coordination forming layers of composition MX_2 separated by van der Waals gaps between the *X* anions. The structures differ in how the layers are stacked. The CdI_2 structure type has AA stacking with one layer per unit cell, and the *X* anions adopt a hexagonal close packed arrangement. The $CdCl_2$ structure has ABC stacking with three layers per unit cell, and the *X* anions adopt a cubic close packed arrangement.

Figure 1 also shows sections of the periodic table highlighting the transition metals for which the MX_2 compounds listed in Table 1 form. Note that compounds with stoichiometry MX_2 are known for other *M*, for example Cr, Mo, and Pd, but they form molecular (cluster) compounds or 1D chain structures. Among the dichlorides, the $CdCl_2$ structure is found only for the later transition metals, and only for Ni in the dibromides and diiodides. However, Schneider et al. have shown that $MnBr_2$ may undergo a crystallographic phase transition from the CdI_2 structure type to the $CdCl_2$ structure type at high temperature [40]. NiI_2 undergoes a crystallographic phase transition at 60 K [41]. It is monoclinic below this temperature, resulting from a slight distortion ($\beta = 90.2°$) from the C-centered orthorhombic description of the hexagonal lattice. In addition, diffraction measurements on $FeCl_2$ under pressure have shown a transition from the $CdCl_2$ structure to the the CdI_2 structure near 0.6 GPa [42,43].

Interatomic distances between *M* cations within the layers and the spacing of the layers are shown in Table 1. For the $CdCl_2$ and CdI_2 structure types the in-plane $M - M$ distance is equal to the length of the crystallographic *a* axis (hexagonal settings). The layer spacing, defined as the distance between the midpoints of neighboring layers measured along the stacking direction, is equal to the length of the *c* axis in the CdI_2 structure and $c/3$ in the $CdCl_2$ structure. Moving across the series from Mn to Ni, both of these distances generally decrease, while less systematic behavior is seen for TiX_2 and VX_2.

Table 1. Summary of structural and magnetic data for layered MX_2 compounds with partially filled *d*-shells. A * indicates that the compound is known to undergo a crystallographic phase transition above or below room temperature. "Magnetic order" refers to long range 3D magnetic order, and is given as antiferromagnetic (AFM), ferromagnetic (FM), or helimagnetic (HM). "Moments in layer" refers to the arrangement of the magnetic moments within a single layer, with || and ⊥ indicating whether the moments are directed parallel to the plane of the layer (in plane) or perpendicular to it (out of plane), respectively. Ordering temperatures (T_N) and Weiss temperatures (θ) are given. References for the magnetic data can be found in the associated text.

Compound	Structure Type	Reference	in Plane $M-M$ Distance (Å)	Layer Spacing (Å)	Magnetic Order	Moments in Layer	T_N, (K)	θ, (K)
$TiCl_2$	CdI_2 ($P\bar{3}m1$)	[44]	3.56	5.88	AFM	–	85	−702
$TiBr_2$	CdI_2 ($P\bar{3}m1$)	[45]	3.63	6.49	–	–	–	–
TiI_2	CdI_2 ($P\bar{3}m1$)	[46]	4.11	6.82	–	–	–	–
VCl_2	CdI_2 ($P\bar{3}m1$)	[47]	3.6	5.83	AFM	120°	36	−565, −437
VBr_2	CdI_2 ($P\bar{3}m1$)	[46]	3.77	6.18	AFM	120°	30	−335
VI_2	CdI_2 ($P\bar{3}m1$)	[48]	4.06	6.76	AFM	–	16.3, 15	−143
$MnCl_2$	$CdCl_2$ ($R\bar{3}m$)	[49]	3.71	5.86	AFM or HM	stripe or HM	2.0, 1.8	−3.3
$MnBr_2$ *	CdI_2 ($P\bar{3}m1$)	[50]	3.89	6.27	AFM	stripe ||	2.3, 2.16	–
MnI_2	CdI_2 ($P\bar{3}m1$)	[51]	4.16	6.82	HM	HM	3.95, 3.8, 3.45	–
$FeCl_2$	$CdCl_2$ ($R\bar{3}m$)	[52]	3.6	5.83	AFM	FM ⊥	24	9 (||), 21 (⊥)
$FeBr_2$	CdI_2 ($P\bar{3}m1$)	[53]	3.78	6.23	AFM	FM ⊥	14	−3.0 (||), 3.5 (⊥)
FeI_2	CdI_2 ($P\bar{3}m1$)	[54]	4.03	6.75	AFM	stripe ⊥	9	24 (||), 21.5 (⊥)
$CoCl_2$	$CdCl_2$ ($R\bar{3}m$)	[55]	3.54	5.81	AFM	FM ||	25	38
$CoBr_2$	CdI_2 ($P\bar{3}m1$)	[56]	3.69	6.12	AFM	FM ||	19	–
CoI_2	CdI_2 ($P\bar{3}m1$)	[51]	3.96	6.65	HM	HM	11	–
$NiCl_2$	$CdCl_2$ ($R\bar{3}m$)	[57]	3.48	5.8	AFM	FM ||	52	68
$NiBr_2$	$CdCl_2$ ($R\bar{3}m$)	[58]	3.7	6.09	AFM, HM	FM ||, HM	52, 23	–
NiI_2 *	$CdCl_2$ ($R\bar{3}m$)	[59]	3.9	6.54	HM	HM	75	–
$ZrCl_2$	MoS_2 ($R3m$)	[60]	3.38	6.45	–	–	–	–
ZrI_2	$MoTe_2$ ($P2_1/m$)	[61]	3.18, 3.74, 4.65	7.43	–	–	–	–
ZrI_2	WTe2 ($Pmn2_1$)	[62]	3.19, 3.74, 4.65	7.44				

The layered phases are restricted to the first row of the transition metals, with the exception of the 4*d* element Zr. Both $ZrCl_2$ and ZrI_2 are reported, but not the dibromide. The zirconium compounds are found to have different structures than the layered 3*d* transition metal dihalides. As shown in Figure 2, $ZrCl_2$ adopts the MoS_2 structure type [60], which has the same triangular nets of metal cations and ABC stacking found in $CdCl_2$. However, in $ZrCl_2$ the Zr atoms are in trigonal prismatic coordination rather than octahedral coordination. As a result the Cl anions do not form a cubic close packed arrangement in $ZrCl_2$ but instead an AABBCC stacking sequence. ZrI_2 is reported to adopt both the $MoTe_2$ and WTe_2 structure types [61,62]. The closely related structures are shown in Figure 2. The regular triangular net of *M* cations found in the compounds described previously is disrupted in ZrI_2, which has zigzag chains of Zr atoms (see $M - M$ in-plane distances in Table 1). This points to the tendency of heavier (4*d* and 5*d*) transition metals to form metal-metal bonds. Indeed, in addition to the layered MoS_2 structure described above for $ZrCl_2$, a molecular crystal structure with Zr_6 clusters is also known [63]. Further examples of this tendency will be noted later in discussion of MX_3 compounds.

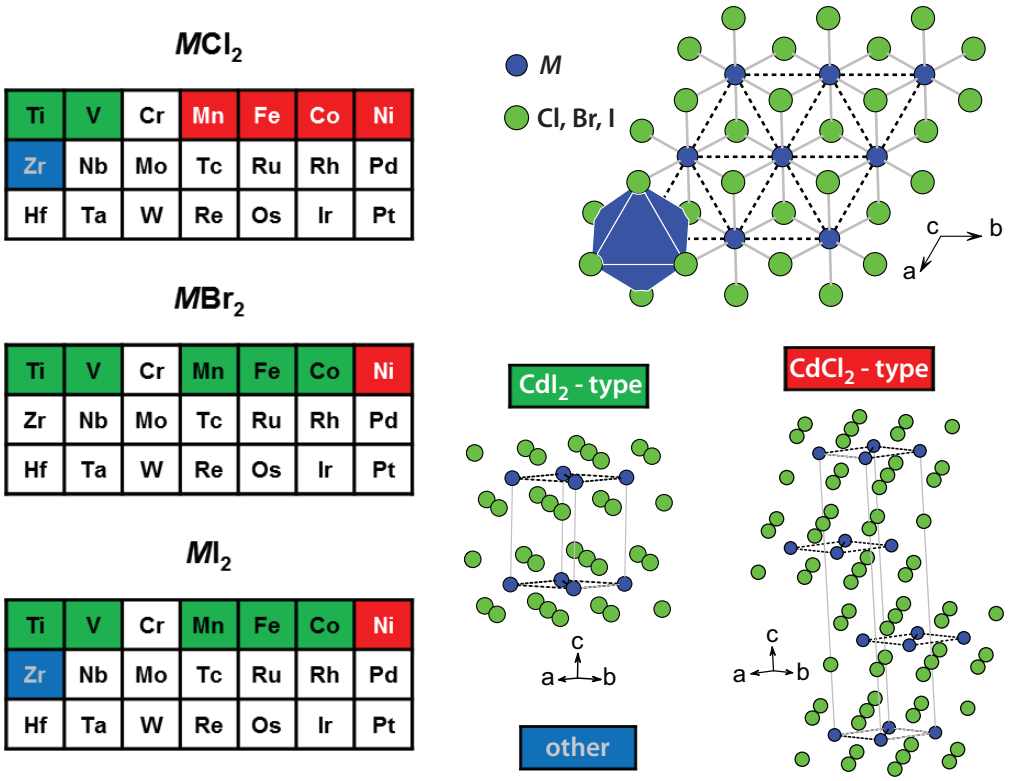

Figure 1. A section of the periodic table showing the transition metals for which layered MX_2 compounds listed in Table 1 form. The metals are highlighted with colors that correspond to the structure types shown on the lower right. A plan view of a single layer common to both the CdI_2 and $CdCl_2$ structure types is shown on the upper right.

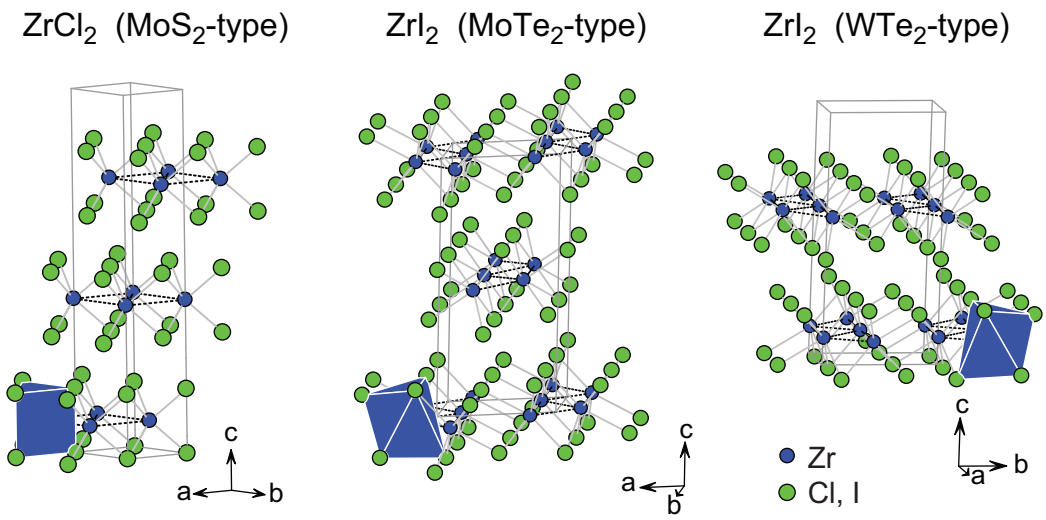

Figure 2. Crystal structures of layered ZrX_2 compounds. A single Zr coordination polyhedron is shown for each structure.

2.2. MX_3 Compounds

Crystal structure information for layered MX_3 compounds is collected in Table 2. Only compounds with transition metals containing partially filled *d*-shells are included, since those are the materials in which magnetism may be expected. Non-magnetic, layered trihalides of Sc and Y, with valence electronic configurations $3d^0$ and $4d^0$, respectively, are also known [28,64–68]. Note that several of these materials also form in 1D chain structures, but those polymorphs are outside of the scope of the present work. All of the layered compounds have been reported to adopt either the monoclinic $AlCl_3$ structure type or the rhombohedral BiI_3 structure type, and this is indicated for each element on the periodic table sections shown in Figure 3. In these materials the common structural motif is a honeycomb net of *M* cations that are in edge sharing octahedral coordination, as shown in Figure 3. In the BiI_3 structure the layer stacking sequence is strictly ABC, and the stacking in $AlCl_3$ is approximately ABC. In the former case subsequent layers are shifted along one of the $M-M$ "bonds" (to the right in the BiI_3 structure shown in Figure 3), while in the latter case the layers are shifted perpendicular to this direction (into the page in the $AlCl_3$ structure shown in Figure 3).

In the BiI_3 structure the honeycomb net is regular due to the three-fold symmetry. In the $AlCl_3$ structure the honeycomb net can be distorted, and the y-coordinate of the *M* site determines the degree of distortion. This results in two unique in-plane $M-M$ distances (Table 2). In most of the compounds these two distances are seen to be quite similar, that is the honeycomb nets are nearly undistorted. The two exceptions are the heavier transition metal compounds $MoCl_3$ and $TcCl_3$, in which the net is broken into dimers that are separated from one another by a distance about one Angstrom longer than their intradimer distance. Metal-metal bonding in Tc halides including layered (β) $TcCl_3$ is discussed in [69].

Three elements, Ti, Fe, and Ru, are reported to form multiple layered crystal structures with stoichiometry MCl_3 (Table 2). This is indicated by the crosshatching on the table in Figure 3. As noted in Table 2, $TiCl_3$ is also reported to form in the trigonal Ti_3O structure type. This is similar to the BiI_3 structure shown in Figure 3, but with an ABB stacking sequence. This same structure type is also found for one of the $FeCl_3$ polymorphs, which also forms in a third structure type (trigonal, $P\bar{3}$) with twelve honeycomb layers per unit cell and a *c* axis length of 70 Å.

Table 2. Summary of structural and magnetic data for layered MX_3 compounds with partially filled *d*-shells. A * indicates that the compound is known to undergo a crystallographic phase transition above or below room temperature. Multiple reported structure types are listed for some compounds. "Magnetic order" refers to long range 3D magnetic order, and is given as antiferromagnetic (AFM), ferromagnetic (FM), or helimagnetic (HM). "Moments in layer" refers to the arrangement of the magnetic moments within a single layer, with || and ⊥ indicating whether the moments are directed parallel to the plane of the layer (in plane) or perpendicular to it (out of plane), respectively, and "canted" indicating a canting away from either of these directions. Ordering temperatures (T_N, T_C) and Weiss temperatures (θ) are given. References for the magnetic data can be found in the associated text.

Compound	Structure Type	Reference	in Plane $M-M$ Distance (Å)	Layer Spacing (Å)	Magnetic Order	Moments in Layer	T_N or T_C, (K)	θ, (K)
$TiCl_3$ *	BiI_3 ($R\bar{3}$)	[28]	3.53	5.83				
$TiCl_3$ *	Ti_3O ($P\bar{3}1c$)	[70]	3.55	5.86	–	–	–	–
$TiBr_3$ *	BiI_3 ($R\bar{3}$)	[71]	3.74	6.21	–	–	–	–
VCl_3	BiI_3 ($R\bar{3}$)	[28]	3.47	5.78	AFM	–	∼20	−30
VBr_3	BiI_3 ($R\bar{3}$)	[72]	3.7	6.21	–	–	–	–
$CrCl_3$ *	$AlCl_3$ ($C2/m$)	[73]	3.44, 3.44	5.80	AFM	FM ||	15.5, 16.8	27
$CrBr_3$ *	BiI_3 ($R\bar{3}$)	[74]	3.64	6.11	FM	FM ⊥	37	47
CrI_3 *	$AlCl_3$ ($C2/m$)	[16]	3.96, 3.97	6.62	FM	FM ⊥	61	70
$FeCl_3$	BiI_3 ($R\bar{3}$)	[75]	3.50	5.80				
$FeCl_3$	Ti_3O ($P312$)	[76]	3.50	5.80	HM	HM	9–10	−11.5
$FeCl_3$	$FeCl_3$ ($P\bar{3}$)	[76]	3.50	5.81				
$FeBr_3$	BiI_3 ($R\bar{3}$)	[77]	3.69	6.13	AFM	–	15.7	–
$MoCl_3$	$AlCl_3$ ($C2/m$)	[78]	2.76, 3.71	5.99	–	–	–	–
$TcCl_3$	$AlCl_3$ ($C2/m$)	[79]	2.86, 3.60	5.86	–	–	–	–
$RuCl_3$ *	$AlCl_3$ ($C2/m$)	[80]	3.45, 3.45	5.69				
$RuCl_3$ *	Ti_3O ($P312$)	[81]	3.45	5.72	AFM	zig-zag canted	7–8, 13–14	37 (||), −150(⊥)
$RuCl_3$ *	$CrCl_3$ ($P3_112$)	[82]	3.44, 3.45	5.73				
$RhCl_3$	$AlCl_3$ ($C2/m$)	[83]	3.44, 3.43	5.70	–	–	–	–
$RhBr_3$	$AlCl_3$ ($C2/m$)	[84]	3.62, 3.62	6.00	–	–	–	–
RhI_3	$AlCl_3$ ($C2/m$)	[84]	3.91, 3.90	6.45	–	–	–	–
$IrCl_3$	$AlCl_3$ ($C2/m$)	[85]	3.46, 3.45	5.64	–	–	–	–
$IrBr_3$	$AlCl_3$ ($C2/m$)	[86]	3.67, 3.64	6.01	–	–	–	–
IrI_3	$AlCl_3$ ($C2/m$)	[86]	–	6.54	–	–	–	–

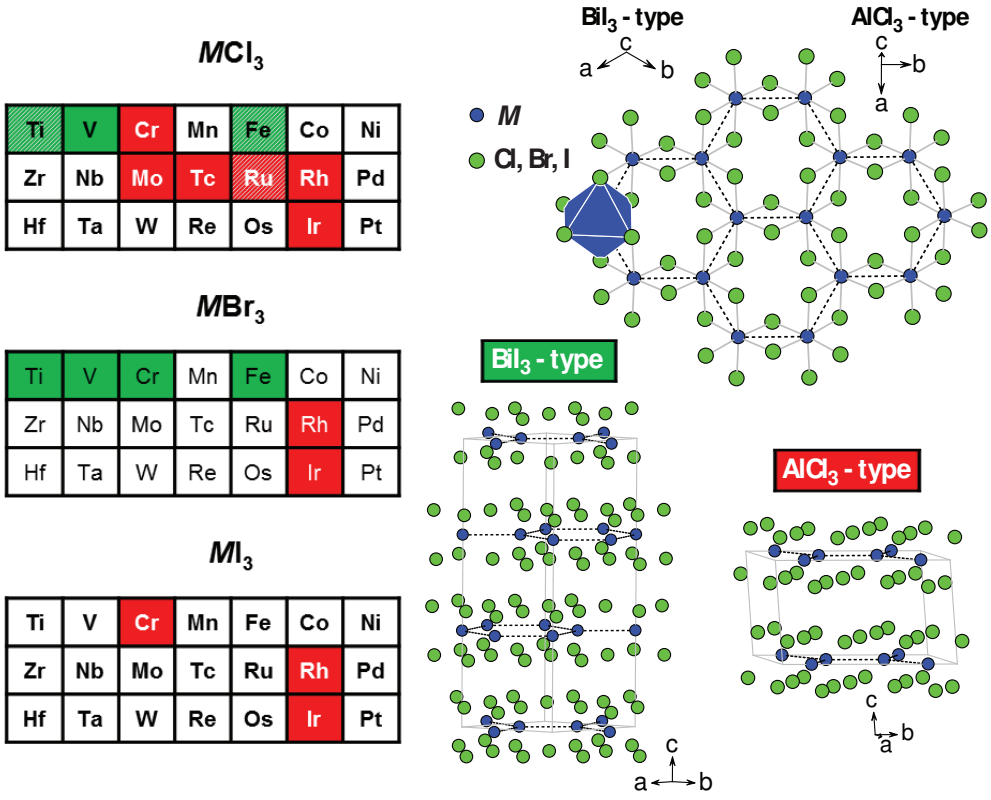

Figure 3. A section of the periodic table showing the transition metals for which layered MX_3 compounds listed in Table 2 form. The metals are highlighted with colors that correspond to the structure types shown on the lower right. Crosshatching indicates multiple structures have been reported (see Table 2). A plan view of a single layer common to both the BiI_3 and $AlCl_3$ structure types is shown on the upper right, with coordinate systems corresponding to each structure type.

$TiCl_3$ undergoes a structural phase transition at low temperature [87]. Troyanov et al. demonstrated that the distortion upon cooling corresponds to a dimerization similar to that noted above in $MoCl_3$ and $TcCl_3$ [70]. Below 220 K a monoclinic structure was reported. The space group, $C2/m$ is the same as the $AlCl_3$ structure type, but the structure is different, with three layers per unit cell. The dimerization is not as extreme in $TiCl_3$ as it is in $MoCl_3$ and $TcCl_3$. At 160 K the Ti-Ti distances within the distorted honeycomb net are 3.36 and 3.59 Å [70], so the dimerization is not as strong at this temperature, 60 K below the transition, as it is in $MoCl_3$ and $TcCl_3$ (Table 2) at room temperature. A structural phase transition is also reported for $TiBr_3$, with a triclinic low temperature structure ($P\bar{1}$) [88], and this same triclinic structure was also later reported for $TiCl_3$ [89].

All three of the layered chromium trihalides are known to undergo temperature induced crystallographic phase transitions between the $AlCl_3$ and BiI_3 structure types [16,73]. At high temperatures all three adopt the $AlCl_3$ structure and transition to the BiI_3 structure upon cooling. This happens near 240, 420, and 210 K in the chloride, bromide, and iodide, respectively. The phase transition is first order, displaying thermal hysteresis and a temperature range over which both phases coexist. Interestingly, it is the lower symmetry monoclinic phase that is preferred at higher temperatures. The transition must be driven by interlayer interactions, since the layers themselves are changed little between the two phases. As expected, twinning and stacking faults develops during the transition upon cooling as the layers rearrange themselves into the BiI_3 stacking, which can complicate interpretation of diffraction data [16].

Multiple structure types have been assigned to the layered form of $RuCl_3$, known as α-$RuCl_3$. Early reports assigned the trigonal space group $P3_112$ [82] (known as the $CrCl_3$ structure type, although

it has been shown that $CrCl_3$ does not actually adopt it) and the $AlCl_3$ type [85], and a tendency to form stacking defects has been noted [86]. The Ti_3O type was also reported [81]. More recently an X-ray and neutron diffraction study reported the monoclinic $AlCl_3$ structure for small single crystals at and below room temperature, and a phase transition in large single crystals from a trigonal structure at room temperature to the monoclinic $AlCl_3$ structure type below about 155 K [80]. A recent report finds high quality crystals undergo a crystallographic phase transition upon cooling from the $AlCl_3$-type at room temperature to the BiI_3-type below about 60 K [90], the same transition described above for CrX_3. Note that even in the monoclinic form the honeycomb net of Ru has little or no distortion (Table 2).

Finally, layered $IrCl_3$ has the $AlCl_3$ structure with a nearly regular honeycomb net (Table 2), but it is also known to adopt a less stable orthorhombic polymorph (*Fddd*). The orthorhombic structure is made up of edge sharing octahedra like the layered structure, but the connectivity extends the structure in three dimensions [91]. It is interesting to note that the structure of orthorhombic $IrCl_3$ is made up of fragments of honeycomb nets like those found in the layered structures shown in Figure 3.

Clearly there are many variants on the stacking sequence in these layered materials due to the weak van der Waals interactions between layers that results in small energy differences between arrangements with different stacking sequences. This is apparent from the crystallographic results from the Ti, Cr, Fe, and Ru trichlorides discussed above. This has been demonstrated using first principles calculations for $RuCl_3$ where multiple structures are found to be very close in energy, and the ground state can depend on the fine details of spin-orbit coupling and electron correlations [92]. The possibility of mechanically separating these materials into thin specimens or even monolayers is of great interest from the point of view of low dimensional magnetism and potential applications and is greatly facilitated by the weakness of the interlayer interactions. The cleavability of several of these compounds has been studied with first principles calculations, using density functionals that incorporate the weak interlayer dispersion forces that are missing from many conventional functionals. For the Ti, V, and Cr trihalides, cleavage energies are reported to be near 0.3 J/m^2, which is smaller than that of graphite [16,17,93]. Stable monolayer crystals of CrI_3 have recently been demonstrated experimentally [21].

3. Magnetic Structures of Layered, Binary, Transition Metal Halides

The magnetic order in layered MX_2 and MX_3 compounds is described below, and some description of the high temperature paramagnetic behavior is given as well. Magnetic excitations and magnetic correlations that develop above the long range ordering temperature are not considered here. Magnetism in these insulating transition metal halide compounds arises from the angular momentum associated with partially filled d orbitals. In octahedral coordination, interaction with the coordinating anions split the five d orbitals into a set of three levels at lower energy, the t_{2g} levels (d_{xy}, d_{xz}, d_{yz}), and two levels at higher energy, the e_g levels ($d_{x^2-y^2}, d_{z^2}$). According to Hund's rules, the d electrons first fill these states singly with their spins parallel, unless the energy cost of putting electrons in the higher energy e_g states overcomes the cost of doubly occupying a single state. In addition to their spin, the electrons in these levels also have orbital angular momentum. In ideal octahedral coordination, the total orbital angular momentum can be shown to be zero for certain electronic configurations. This arises due to rotational symmetry of the system, and when this occurs the orbital angular momentum is said to be "quenched". For octahedral coordination the orbital angular momentum is quenched when there is exactly one electron in each of the t_{2g} orbitals, and when there are two electrons in each of the t_{2g} orbitals. Otherwise there is an orbital moment that must be considered. There is no orbital angular momentum associated with the e_g orbitals. Of course, distortions of the octahedral environments can affect the details of the magnetism that are based on symmetry and degeneracy of electronic states. Despite the partially filled d-orbitals, the materials considered here are electrically insulating under ambient conditions. This can be attributed to a Mott-Hubbard type mechanism by which electron-electron interactions produce a band gap related to the Coulomb repulsion among the well-localized electrons (see for example [94]).

Magnetism in a material is often first characterized by measurements of magnetization (M) as functions of applied magnetic field (H) and temperature (T). Considering magnetic interactions between localized magnetic moments, the temperature dependence of the magnetic susceptibility ($\chi = M/H$) can often be described by the Curie-Weiss formula, $\chi(T) = \mathrm{C}/(T-\theta)$. The Curie constant (C) is a measure of the size of the magnetic moment and is given by $C = \frac{N_A}{3k_B}\mu_B^2 g^2 S(S+1)$, where N_A is Avogadro's number, k_B is the Boltzmann constant, μ_B is the Bohr magneton, S is the total spin, and $g = 2.00$ is the electron gyromagnetic ratio. The "effective moment" (μ_{eff}) is also often quoted, $\mu_{eff} = g\sqrt{S(S+1)}\mu_B$. In cgs units, $\mu_{eff} \approx \sqrt{8\mathrm{C}}$. Fully ordered magnetic moments are expected to be equal to gS in units of Bohr magnetons. When both orbital and spin moments are present, the total angular momentum and associated g-factor must be used. The Weiss temperature (θ) is a measure of the strength of the magnetic interactions. Considering magnetic interactions between nearest neighbors of the form $H_{ij} = -J\overrightarrow{S_i}\cdot\overrightarrow{S_j}$, it can be shown that the Weiss temperature depends on the spin S, the magnetic exchange interaction strength J, and the number of nearest neighbors z according to $\theta = \frac{2zJ}{3k_B}S(S+1)$. Positive values of θ indicate positive values of J, which indicate ferromagnetic interactions. Negative values of θ indicate antiferromagnetic interactions. In a simple mean field model, the Weiss temperature corresponds to the ordering temperature ($T_{C,N} = |\theta|$). Note that the presence of multiple types of interactions, for example FM intralayer interactions and AFM interlayer interactions, complicates the interpretation of Weiss temperatures.

In the materials considered here, the in-plane magnetic interactions between transition metal cations are expected to arise mainly from superexchange through shared coordinating halogen anions. The sign of the superexchange interaction depends upon many factors, including the orbital occupations and the $M-X-M$ angle (see, for example, the discussion in [94]). It is often AFM and strong when the angle is 180°. When this angle is 90°, as it is in the edge sharing octahedral coordination found in layered MX_2 and MX_3 compounds, superexchange can be either FM or AFM. There are also direct $M-M$ exchange interactions, which tend to be AFM, but this is expected to be relatively weak in these materials due to the relatively large $M-M$ distances. The in-plane magnetic order in most of the compounds described below either is ferromagnetic, contains ferromagnetic stripes, or has a helimagnetic arrangement. The later two scenarios are expected to arise from competing magnetic interactions. The exceptions are VX_2 in which the interactions are predominantly AFM [95], and perhaps $TiCl_2$.

Note that in the figures below showing the magnetic structures of MX_2 and MX_3 compounds, only the M sublattices are shown. The magnetic moments directions are indicated by red arrows. In addition, to make the magnetic structures easier to view, different colored balls are used to represent atoms with moments along different directions, except for in the more complex helimagnetic structures.

3.1. MX_2 Compounds

3.1.1. TiX_2 and ZrX_2

These compounds have Ti and Zr in the unusual formal oxidation state of 2+. However, as noted above, metal-metal bonds are present in ZrI_2, so this simple electron counting is invalid in this case. Divalent Ti and Zr in TiX_2 and $ZrCl_2$ have electron configurations of $3d^2$ and $4d^2$, respectively, with an expected spin of $S = 1$. There have been very few magnetic studies of these materials, likely due in part to their instability and reactivity. Magnetic susceptibility measurements on $TiCl_2$ down to 80 K have revealed a cusp near 85 K [96]. The authors suggest that this may indicate antiferromagnetic ordering at this temperature, although they note that previous measurements showed smoothly increasing susceptibility upon cooling from 300 to 20 K [97], but this was based on only six temperature points and significant features could have been overlooked. Magnetic susceptibility versus temperature curves have somewhat unusual shapes, and effective moments of 1.1 and 2.0 μ_B per Ti have been reported [96,97]. A Weiss temperature of −702 K was determined by Starr et al. [97], which would

indicate strong antiferromagnetic interactions. Frustration of these interactions by the triangular Ti lattice may be responsible for the relatively low ordering temperature of 85 K proposed in Ref. [96].

$ZrCl_2$ is reported to have a reduced magnetic moment at room temperature [96], but no temperature dependent data were reported. The authors suggest that this may indicate strong antiferromagnetic interactions between Zr magnetic moments. No magnetic structure determinations for $TiCl_2$ were located in the literature and no magnetic information was found for $TiBr_2$ or TiI_2.

3.1.2. VX_2

These materials contain divalent V with an electronic configuration $3d^3$, $S = 3/2$. An early report on VCl_2 found it to be paramagnetic with a large negative Weiss temperature (−565 K) indicating strong antiferromagnetic interactions [97]. Niel et al. later reported Weiss temperatures of −437, −335, and −143 K for VCl_2, VBr_2, and VI_2, respectively, with effective moments close to the expected value of 3.9 μ_B, and explained their behavior in terms of a 2D Heisenberg model [95].

A neutron powder diffraction study showed that all three of the vanadium dihalides order antiferromagnetically with Néel temperatures of 36.0 K for VCl_2, 29.5 K for VBr_2 and 16.3 K for VI_2 [98]. The strong suppression of these ordering temperatures relative to the Weiss temperatures is a result of geometrical frustration. Both temperatures trend to lower values as the halogen is changed from Cl to Br to I. Further neutron scattering experiments revealed that the magnetic order in VCl_2 develops in two steps, with phase transition temperatures separated by about 0.1 K, and found the magnetic structure at low temperature to be a 120° Néel state shown in Figure 4, where each moment in the triangular lattice is rotated by this angle with respect to its neighbors, with moments in the *ac*-plane [2]. The ordered moment corresponded to a spin of 1.2. In that study, three types of critical behavior were observed, corresponding to 2D Heisenberg, 3D Heisenberg, and 3D Ising models. A similar magnetic structure was found for VBr_2 with moments of about 83% of the expected value [99]. The magnetic order in VI_2 develops in two steps with $T_{N1} = 16.3$ K and T_{N2} near 15 K, but the low temperature magnetic structure of this compound was not resolved with any certainty [98].

Recently Abdul Wasey et al. proposed VX_2 materials as promising candidates for extending 2D materials beyond graphene and dichalcogenides [100]. They report results of first principles calculations of the magnetic order in these systems in both bulk and monolayer forms. In the bulk crystal the experimental spin structure was reproduced. A similar structure is predicted for the monolayer, and the authors suggest that magnetic order in the monolayer may occur at much higher temperature than in the bulk.

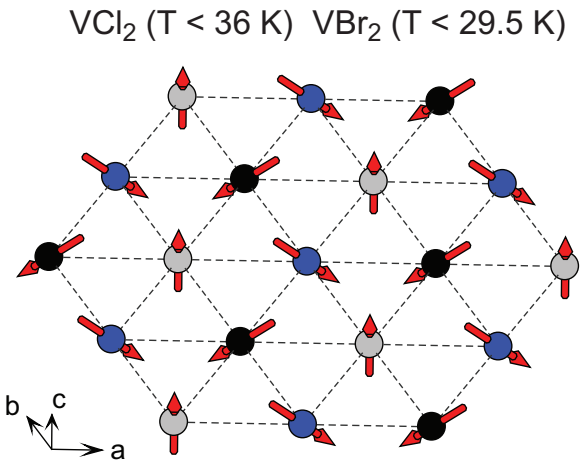

Figure 4. The 120° magnetic structure determined for VCl_2 and VBr_2. The image shows a single triangular net of V atoms lying in the *ab* plane. Moments on the grey atoms are along the *c* axis. Moments on the black and blue atoms lie in the *ac* plane and are rotated by an angle of ±120° from the *c* axis.

3.1.3. MnX_2

Divalent Mn has a $3d^5$ electronic configuration, with $S = 5/2$. Magnetization measurements for $MnCl_2$ indicate weak antiferromagnetic interactions ($\theta = -3.3$ K) and an effective moment of 5.7 μ_B, close to the expected value of 5.9 μ_B [97]. Heat capacity measurements indicate magnetic phase transitions at 1.96 and 1.81 K [101]. The magnetic structures of $MnCl_2$ below these two transitions have not been completely determined. Neutron diffraction from single crystals were analyzed assuming a collinear structure and complex orderings with stripes of ferromagnetically aligned spins in the plane were proposed [102]. A more recent investigation of $MnCl_2$-graphite intercalation compounds found that the magnetic order within isolated $MnCl_2$ layers could be described by an incommensurate helimagnetic arrangement, and it was suggested that this may also hold for the magnetic structure of the bulk crystal [103].

A heat capacity anomaly was reported at 2.16 K in $MnBr_2$, and neutron diffraction showed that antiferromagnetic order is present below this temperature [50]. The magnetic structure has ferromagnetic stripes within the layers with antiferromagnetic coupling between neighboring stripes, as depicted in Figure 5. The moments are along the *a* axis of the hexagonal cell of the crystal structure. There is antiferromagnetic order between the layers. Later, an incommensurate magnetic phase was identified between this phase and the paramagnetic state, persisting up to about 2.3 K [104].

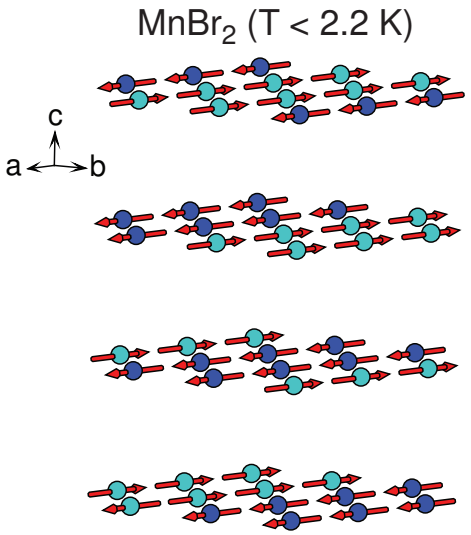

Figure 5. The lowest temperature, commensurate magnetic structure of $MnBr_2$. The coordinate system refers to the underlying hexagonal crystal structure. Dark blue is used for Mn atoms with moments along the hexagonal *a* direction, and light blue for those with moments along -*a*.

MnI_2 adopts a complicated helical magnetic structure below 3.4 K [105]. The moments lie in the (307) planes, and are ferromagnetically aligned within each of these planes. The variation of the moment direction upon moving between (307) planes was originally reported to be a rotation by $2\pi/16$ [105]. Further measurements resolved multiple phase transitions as the magnetic order develops and find the helical ordering to be incommensurate, but with a wave vector close to that reported in the earlier work [104].

It was recently noted that a ferroelectric polarization develops in the magnetically ordered state of MnI_2, spurring interest in this compound as a multiferroic material [6,7]. Density functional theory calculations suggest that spin-orbit coupling on the iodine ions is the main source of the ferroelectric polarization in MnI_2 [7], which has been measured to exceed 120 $\mu C/m^2$ [6]. While spin-orbit coupling is required to accurately describe the polarization, is was found to have little influence on the magnetic interactions determined by fitting density functional theory results to a Heisenberg model [7]. In that study it was found that the observed helimagnetic order arises from

competing magnetic interactions on the triangular Mn lattice, that electronic correlations, which weaken AFM superexchange, must be considered to accurately reproduce the experimental magnetic structures, and that the details of the spiral structure are sensitive to relatively strong interplane magnetic interactions. The ferroelectric polarization responds to applied magnetic fields in multiferroic MnI_2. Magnetic fields affect the polarization by modifying the helimagnetic domain structure at low fields, and by changing the magnetic order at higher fields [6]. Ferroelectric distortions onsetting at the magnetic ordering temperatures and associated multiferroictiy is a common occurrence in MX_2 compounds that adopt non-collinear magnetic structures (see CoI_2, $NiBr_2$, and NiI_2 below); however, the details of the coupling between the spin and electric polarization in these and related triangular lattice multiferroics is not well understood [8].

3.1.4. FeX_2

The divalent iron, $3d^6$, in these compounds is expected to be in the high spin state with $S = 2$. The partially filled t_{2g} levels means that orbital angular momentum is not quenched, and an orbital moment may be expected, as discussed in [106] and references therein. Significant anisotropy is observed in the paramagnetic state in all three of the iron dihalides, with a larger effective moment measured along the c axis [107]. Moments in the magnetically ordered states are also along this direction. Weiss temperatures determined from measurements with the field in the plane ($||$) and out of the plane ($\perp$) are 9 K ($||$) and 21 K ($\perp$) for $FeCl_2$, -3.0 K ($||$) and 3.5 K ($\perp$) for $FeBr_2$, and 24 K ($||$) and 21.5 K ($\perp$) for FeI_2 [107].

Although the crystallographic structures of $FeCl_2$ and $FeBr_2$ differ (Table 1), they have the same ordered arrangement of spins at low temperature. This magnetic structure is shown in Figure 6, and contains ferromagnetic intralayer order and antiferromagnetic stacking. The chloride orders below 24 K and has an ordered moment of 4.5 μ_B [108], and the bromide orders below 14 K and has an ordered moment of 3.9 μ_B [108,109]. The iodide adopts a different low temperature structure below its Néel temperature of 9 K, with two-atom-wide ferromagnetic stipes in the plane (ordered moment of 3.7 μ_B) that are aligned antiferromagnetically with neighboring stripes [54]. The moment arrangement is shifted from layer to layer so that the magnetic unit cell contains four layers. This is similar to the magnetic structure of $MnBr_2$ shown in Figure 5, but the stripes run in different directions in the plane. There is no apparent correlation between the Weiss temperatures and magnetic ordering temperatures in the FeX_2 series. This is likely related to the presence of both FM and AFM interaction in these materials, which complicates interpretation of the fitted Weiss temperatures.

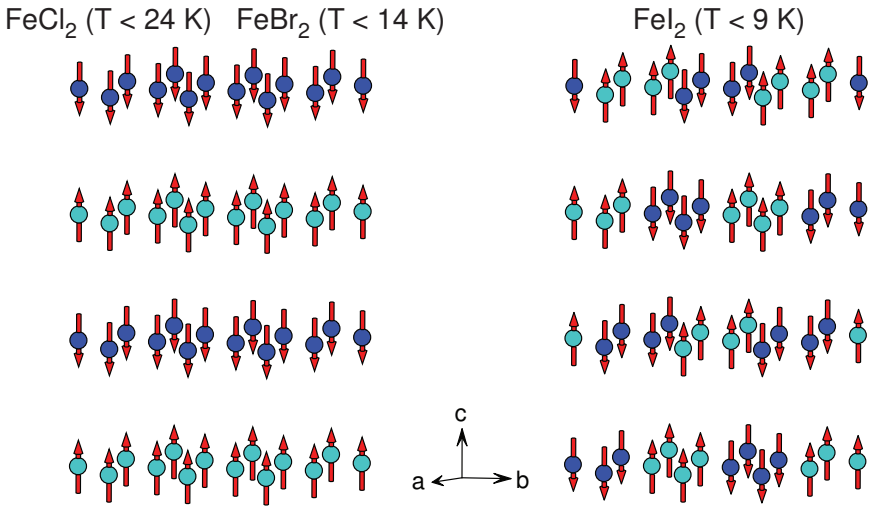

Figure 6. The magnetic structures of FeX_2 with the hexagonal coordinate system of the underlying crystal lattice shown. All moments are along either the +c or -c direction.

As noted above, $FeCl_2$ undergoes a transition from the $CdCl_2$ structure to the CdI_2 structure at a pressure of 0.6 GPa. At higher pressures two additional phase transitions occur, with pronounced effects on the magnetic behavior. Above 32 GPa the orbital moment is quenched and the magnetic moments cant away from the *c* axis. A further increase in pressure results in the collapse of the magnetization and an insulator-metal transition that is attributed to delocalization of the Fe *d* electrons [43,110]. Similar behavior is reported for FeI_2 [111]. In both materials the Néel temperature in increased with applied pressure, and reaches room temperature before collapsing into the non-magnetic state.

In the antiferromagnetic state, magnetic field induced phase transitions, or metamagnetic transitions, occur in $FeCl_2$, $FeBr_2$, and FeI_2 at applied fields near 11, 29, and 46 kOe, respectively [109,112,113]. This arises from stronger ferromagnetic coupling within the layers compared to the weak antiferromagnetic coupling between them, and led to much of the early interest in these materials, as summarized in [114] and references therein. The most complex behavior is seen in FeI_2 [113]. From magnetization and heat capacity measurements, Katsumata et al. identified four different field induced phases, in addition to the antiferromagnetic ground state, and proposed ferrimagnetic structures for them [106]. In addition, Binek et al. have proposed the emergence of a Griffith's phase in $FeCl_2$ [115,116], and neutron diffraction has been used to construct the temperature-field magnetic phase diagram of $FeBr_2$ [117].

3.1.5. CoX_2

Cobalt dihalides have cobalt in electronic configuration $3d^7$, which can have a high ($S = 3/2$) or low ($S = 1/2$) spin state. Orbital magnetic moments may be expected in either state. It is apparent from neutron diffraction results that the high spin state is preferred, at least for $CoCl_2$ and $CoBr_2$. The ordered moment on Co in $CoCl_2$ which orders below 25 K [118], is 3.0 μ_B [108], and it is 2.8 μ_B in $CoBr_2$ [108], which orders at 19 K [119]. These are close to the expected value of gS for $S = 3/2$ for high-spin only. However, magnetization measurements on $CoCl_2$ [97] indicate an enhanced effective moment in the paramagnetic state (5.3 μ_B), which suggests an orbital contribution, and a Weiss temperature of 38 K.

Below their ordering temperatures, both of these compounds adopt the magnetic structure shown in Figure 7, with ferromagnetic alignment within each layer and antiferromagnetic stacking. The moments are known to be parallel or antiparallel to the hexagonal [210] direction for $CoCl_2$ [108], as shown in the Figure. The moments in $CoBr_2$ are only known to lie within the *ab* plane [108].

The magnetic behavior in CoI_2 is more complex. CoI_2 is a helimagnet with a spiral spin structure, and anisotropic magnetic susceptibility in the paramagnetic state arising from spin-orbit coupling [120]. Powder neutron diffraction analysis indicated a cycloidal structure with moments in the plane and planes stacked antiferromagnetically [41], which is supported by Mössbauer spectroscopy [121]. The corresponding in-plane spin arrangement is shown Figure 7. Mekata et al. used single crystal neutron diffraction to examine the magnetic order in CoI_2 and found evidence of a more complicated magnetic structure that requires an additional propagation vector to describe. The same study identified a first order magnetic phase transition at 9.4 K, just below the magnetic ordering transition at 11.0 K, and suggested that these successive transitions may arise due to in-plane magnetic frustration, but no change in the magnetic structure was observed at 9.4 K [120].

An electric polarization of about 10 $\mu C/m^2$ that varies with applied magnetic field is induced below the magnetic ordering transition in CoI_2 indicating multiferroic behavior [8] (see MnI_2 above, $NiBr_2$, NiI_2 below).

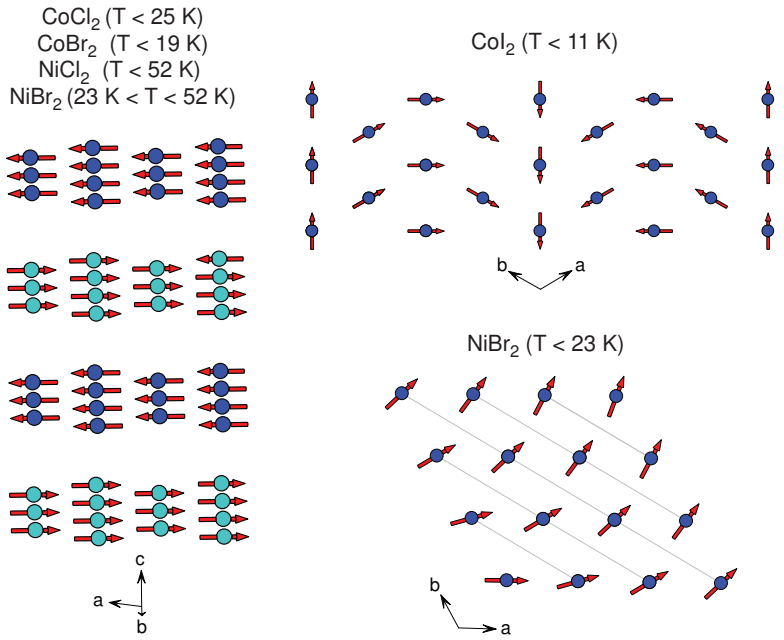

Figure 7. Magnetic structures of CoX_2 and NiX_2 for X = Cl and Br, and CoI_2. The moments lie in the plane in each case, and are known to be parallel and antiparallel to the [210] direction in the commensurate structures of $CoCl_2$ and NiX_2. A layer of the commensurate, cycloidal, helimagnetic structure of CoI_2 reported in [41] is shown. A more complex cycloidal structure has also been reported [120]. Only a small portion of one layer of the lower temperature (T < 23 K) long period helimagnetic structure of $NiBr_2$ is shown. Coordinate systems of the hexagonal crystallographic unit cells shown for reference.

3.1.6. NiX_2

The octahedrally coordinated, divalent nickel in these compounds has a $3d^8$ electronic configuration, with filled t_{2g} and half-filled e_g orbitals. Magnetic moments are expected to be spin only, as orbital angular momentum is quenched in this configuration. Magnetization data for $NiCl_2$ indicate an effective moment of 3.3 μ_B, somewhat larger than the spin only value of 2.8 μ_B expected for $S = 1$, and Weiss temperature of 68 K, suggesting predominantly ferromagnetic interactions [97]. The Néel temperatures of $NiCl_2$ and $NiBr_2$ are quite similar; upon cooling, both develop long range antiferromagnetic order below 52 K [122,123]. Their fully ordered moments are 2.11 and 2.0 μ_B, respectively [123,124], as expected for $S = 1$. The resulting magnetic structure is shown in Figure 7a. The moments lie within the ab plane and are ferromagnetically aligned within each layer, with antiferromagnetic stacking. The moment directions were determined from Mössbauer spectroscopy to be parallel and antiparallel to the [210] direction, as depicted in the figure [125].

While the magnetic structure shown in Figure 7 describes $NiCl_2$ at all temperatures below T_N, $NiBr_2$ undergoes a second phase transition, to a more complicated magnetic structure below 23 K [123,126,127]. Below this first order transition the magnetic moments adopts an incommensurate helimagnetic structure with a periodicity that varies with temperature. As described by Adam et al., the magnetic moments still lie within the basal plane, but vary in direction at 4.2 K by 9.72° from site to site along both the hexagonal a and b axes [123], as depicted in Figure 7. This results in a periodicity of about 37 crystallographic unit cells along each in-plane direction. The stacking remains antiferromagnetic.

Heat capacity data show that NiI_2 undergoes two phase transitions upon cooling, at 75 and 60 K [128]. Helimagnetic order develops at 75 K, and the phase transition at 60 K is crystallographic [41]. The helimagnetic structure of NiI_2 is incommensurate with the nuclear structure and the moments

rotate in a plane that makes a 55° angle with the *c* axis, as depicted in [41]. The ordered moment at 4.2 K was determined to be 1.6 μ_B.

Like helimagnetic MnI_2 and CoI_2 described above, $NiBr_2$ and NiI_2 also develop a ferroelectric polarization in their helimagnetic states [5,8]. Polarizations of 20–25 $\mu C/m^2$ are observed in the bromide, and polarizations exceeding 120 $\mu C/m^2$ are reported for the iodide. As in MnI_2 and CoI_2, the polarization can be controlled by applied magnetic fields through their influence on the helimagnetic domain structure [5,8].

3.2. MX_3 Compounds

Several of the MX_3 compounds listed in Table 2 are not known to form magnetically ordered states. These include TiX_3, $MoCl_3$, $TcCl_3$, RhX_3, and IrX_3. The later two materials have electron configuration $4d^6$, and are expected to have non-magnetic ground states with all electrons paired. A clue to the non-magnetic nature of $MoCl_3$ [78] is found in the magnetic behavior of $TiCl_3$. Although neutron diffraction shows no magnetic ordering in layered $TiCl_3$ at low temperature, magnetic susceptibility shows a dramatic and sharp decrease near 217 K. This corresponds to the structural distortion noted above in the discussion of $TiCl_3$ and described in [70,89]. Ogawa had earlier observed a lattice response coincident with the magnetic anomaly, and proposed that the formation of covalently bonded Ti-Ti dimers that pair the *d* electrons on each Ti as the reason for the collapse of the magnetic moment [87]. Thus the strong dimerization in $MoCl_3$ (Table 2) is expected to be responsible for its non-magnetic nature. Dimerized $TcCl_3$ is also expected to be non-magnetic [69].

3.2.1. VX_3

Little information about magnetic order in VCl_3 or VBr_3 is available. These compounds are expected to be magnetic due to their electron configuration $3d^2$ ($S = 1$) and the undistorted honeycomb net of the BiI_3 structure type reported for these materials (Table 2). Magnetic susceptibility data [97] for VCl_3 give an effective moment of 2.85 μ_B, close to the expected value for $S = 1$ (2.82 μ_B), and a Weiss temperature of −30 K, indicating antiferromagnetic interactions. The maximum displayed near 20 K in the temperature dependence of the susceptibility suggests antiferromagnetic order at lower temperatures. First principles calculations have been done to examine the electronic and magnetic properties of monolayers of VCl_3 and (hypothetical) VI_3 [93,129]. Both are predicted to be ferromagnetic.

3.2.2. CrX_3

In these compounds Cr is expected to be in a $3d^3$ electronic configuration, and effective moments determined from high temperature magnetic susceptibility range from 3.7 to 3.9 μ_B per Cr as expected for $S = 3/2$ [16,97,130]. Weiss temperatures determined from these measurements are 27, 47, and 70 K for $CrCl_3$, $CrBr_3$, and CrI_3, respectively, indicating predominantly ferromagnetic interactions. In fact, among the layered MX_2 and MX_3 materials, the chromium trihalide family contains the only compounds in which long-range, 3D ferromagnetic ground states are observed. The magnetic structures are shown in Figure 8. Below 61 K for CrI_3 and 37 K for $CrBr_3$, moments directed out of the plane order ferromagnetically [16,130–132]. In $CrCl_3$ below about 17 K, ferromagnetic order is also observed within the layers, but the layers stack antiferromagnetically [133,134]. Also unlike the tribromide and triiodide, the moments in $CrCl_3$ lie within the planes. In this series, the ordering temperatures scale nicely with the Weiss temperatures. The ordered moments determined by neutron diffraction and magnetic saturation are all close to 3 μ_B as expected for the $3d^3$ electronic configuration of Cr^{3+}. Reported values are 2.7–3.2 μ_B for $CrCl_3$ [133], 3 μ_B for $CrBr_3$ [130], and 3.1 $\mu_B$for CrI_3 [16,132]. Significant magnetic anisotropy is observed in the ferromagnetic state of CrI_3; the anisotropy field, the field required to rotate the ordered moments away from the *c*-axis and into the *ab*-plane, is found to be near 30 kOe near 2 K [16,132]. Ferromagnetic $CrBr_3$ has a significantly lower anisotropy field of about 5 kOe [130,131].

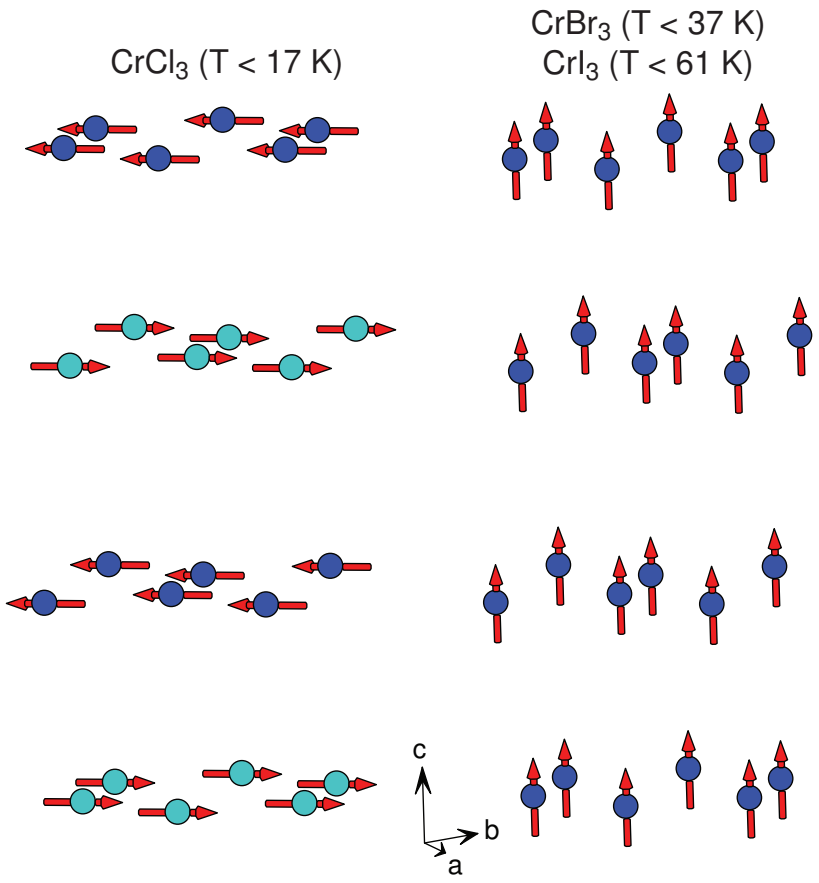

Figure 8. Magnetic structures of CrX_3. The hexagonal coordinate system of the low temperature rhombohedral structure is shown. The moments in $CrCl_3$ are drawn along the [110] and [$\bar{1}\bar{1}$0] directions here, but are only known to be in the *ab* plane. Moments are along the *c* axis in ferromagnetic $CrBr_3$ and CrI_3.

With moments in the plane and antiferromagnetic stacking of the layers $CrCl_3$ is unique among the chromium trihalides. It also has weak magnetic anisotropy. A magnetic field of only a few kOe is sufficient to overcome the antiferromagnetic order and fully polarize the magnetization in any direction [133,134]. Using the optical technique of Faraday rotation, Kuhlow followed closely the evolution of the magnetization in $CrCl_3$ with changing temperature and applied magnetic field [134]. It was noted that the magnetic order appears to onset in two stages upon cooling, first developing ferromagnetic correlations and 16.7 K with long range antiferromagnetic order as shown in Figure 8 below 15.5 K.

The ferromagnetism in these CrX_3 compounds makes them particulary interesting for incorporating magnetism into functional van der Waals heterostructures. Several relevant theoretical studies have been reported that suggest ferromagnetic order may persist into monolayer specimens [15–18]. Recently ferromagnetic monolayers of CrI_3 were demonstrated experimentally [21]. Ferromagnetic CrI_3 was also recently incorporated into a van der Waals heterostructure in which an exchange field effect equivalent to a 13 T applied magnetic field was observed in the electronic properties of monolayer WSe_2 when the heterostructure was cooled through the Curie temperature of CrI_3 [20]. Although $CrCl_3$ has an antiferromagnetic structure in the bulk, each layer is ferromagnetically ordered. If this proves to be independent of sample thickness then ferromagnetic monolayers may be realized in all three of the chromium trihalides, with a range of magnetic anisotropy that may allow easy tuning of the magnetization direction in the chloride or more robust moment orientation in the iodide.

3.2.3. FeX_3

$FeCl_3$ and $FeBr_3$ have iron in the $3d^5$ configuration. There has been considerable study of the magnetism in the chloride, but very little for the bromide. Early magnetization measurements on $FeCl_3$ found an effective moment of 5.7 μ_B, close to the expected spin-only value of 5.9 μ_B, and a Weiss temperature of -11.5 K, indicating antiferromagnetic interactions [97]. A neutron diffraction study found a helimagnetic structure for $FeCl_3$ below about 15 K, with an ordered moment on 4.3 μ_B per iron at 4.2 K [135]. The reduction from the expected value of 5 μ_B may be due to some disorder still present at 4.2 K or could arise from a slight distortion from the periodic model used to describe the magnetic order. Later magnetization measurements place the Néel temperature at 9–10 K [136,137].

The magnetic structure of $FeCl_3$ is shown in Figure 9. The figure shows one layer of Fe atoms, with dashed lines denoting (140) planes. Sites in this layer on a common (140) plane have parallel moments with their orientation indicated at the left of the Figure. Note that the moments all have the same magnitude, but their projections on to the plane of the page vary as their orientations rotate about the [140] direction by $2\pi/15$ between neighboring planes [135]. The layers stack antiferromagnetically. A field induced magnetic phase transition was noted in $FeCl_3$ by Stampfel et al. and Johnson et al. with the magnetic structure evolving with field up to about 15 kOe and experiencing a spin-flop near 40 kOe [137,138]. A Mössbauer spectroscopy study of $FeBr_3$ found magnetic order below 15.7 K, and the authors proposed the order below this temperature to be antiferromagnetic in analogy with $FeCl_3$ [139].

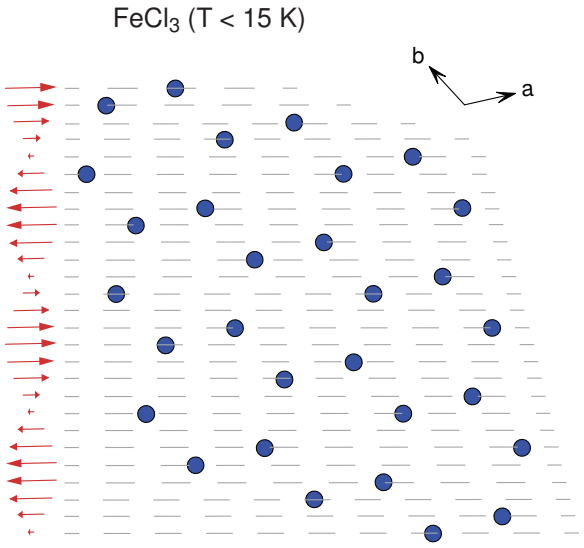

Figure 9. The helimagnetic structure of $FeCl_3$. A portion of one layer of Fe atoms is shown, along with the hexagonal coordinate system. The dotted lines indicate (140) planes. The moment of the atoms lying on these planes is indicated by the red arrows at the left of each line. Moments are in the (140) planes and have components in and out of the page.

3.2.4. RuX_3

Recent interest in $RuCl_3$ began with Plumb et al. identifying it as a spin-orbit assisted Mott insulator in which a small band gap arises from a combination of spin-orbit interactions and strong electron-electron correlations [9]. In this compound, Ru has electron configuration $3d^5$. Considering spin only gives an option of a high spin configuration ($S = 5/2$) with all t_{2g} and e_g levels half filled, or a lower spin configurations with some levels doubly occupied. In this case the crystal field splitting is large enough so that all five of the d electrons go into the lower, t_{2g} set leaving only one unpaired spin ($S = 1/2$). However, the orbital angular momentum is not quenched and cannot be neglected. In addition, the spin orbit coupling interaction, which increases in strength as Z^4 where Z is the atomic

number of the nucleus, must also be considered for this heavy, 4*d* transition metal. In $RuCl_3$, spin orbit coupling, along with significant electron-electron correlations, splits the otherwise degenerate t_{2g} states into states with effective angular momentum $j_{eff} = 3/2$ and $j_{eff} = 1/2$ [10,140]. The $j_{eff} = 3/2$ states are lower in energy, and hold four of the five *d* electrons, leaving one for the higher energy level, and giving Ru in this compound an angular momentum of $j_{eff} = 1/2$. Magnetization measurements in the paramagnetic state have been reported for both powder and single crystals. Powder measurements give effective moments of 2.2–2.3 μ_B and Weiss temperatures of 23–40 K [13,81,141,142]. Single crystal measurements show strong paramagnetic anisotropy, and give $\mu_{eff} = 2.1\,\mu_B$ and $\theta = 37$ K with the field applied in the plane, and $\mu_{eff} = 2.7\,\mu_B$ and $\theta = -150$ K with the field applied perpendicular to the layers [143].

Two magnetic phase transitions have been observed in $RuCl_3$, at 14 K and 7 K. It is believed that the difference depends upon the details of the stacking sequence of the $RuCl_3$ layers and the density of stacking faults [13]. Some crystals show only one transition or the other, while others samples show both. In crystals which undergo no crystallographic phase transition upon cooling (see above) and remain monoclinic at all temperatures magnetic order occurs below 14 K, while crystals that undergo a structural transition upon cooling show only the 7 K transition [13,90]. Pristine crystals that have shown a phase transition at 7 K can be transformed into crystals with only the 14 K transition through mechanical deformation [13,80]. Although all of the details of the magnetic structures of the two phases are have not been settled, there is consensus that the in-plane magnetic structures are of the so-called zig-zag type [11–13,80] shown in Figure 10. Determinations of the size of the ordered moment include $\leq 0.4\,\mu_B$ [13], $\leq 0.45\,\mu_B$ [80], $\geq 0.64\,\mu_B$ [12], and $0.73\,\mu_B$ [90]. The moment direction is reported to lie in the monoclinic *ac*-plane, with components both in and out of the plane of the $RuCl_3$ layers [12,80,90]. The layers stack antiferromagnetically with a different stacking sequence associated with the different transition temperatures. AB magnetic stacking is seen in crystals with a 14 K transition, ABC stacking is seen in crystals with a 7 K transition, and both types of stacking onsetting at the appropriate temperatures are seen in samples with both transitions [12,13,80].

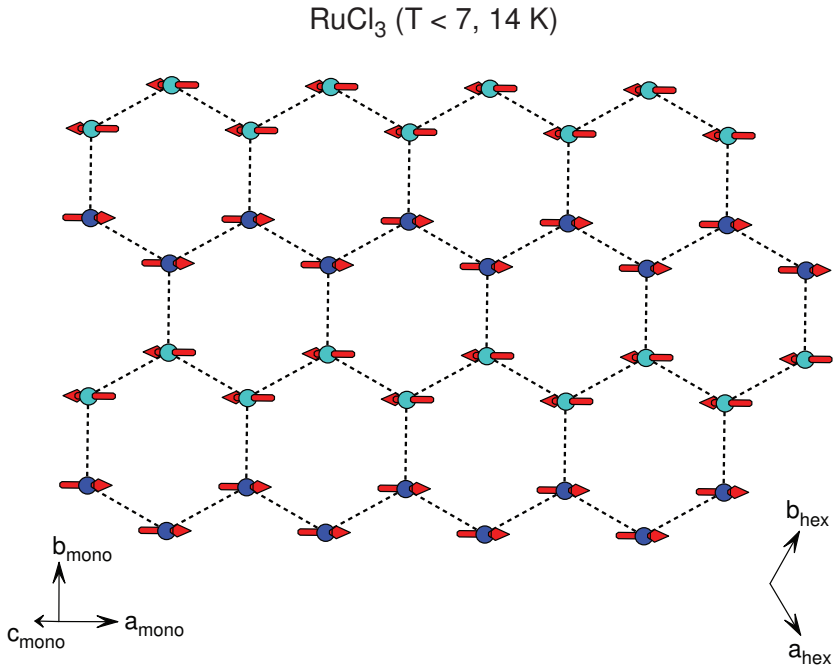

Figure 10. The zig-zag in plane magnetic structure of $RuCl_3$. Coordinate systems corresponding to the underlying monoclinic and hexagonal crystal lattices are shown. The moments lie in the monoclinic *ac* plane, but the direction in this plane is not known well.

With $j_{eff} = 1/2$ and strong spin orbit coupling on a honeycomb lattice, $RuCl_3$ is identified as a promising system for studying the Kitaev model [9,10,144]. In this model, anisotropic interactions result in a type of magnetic frustration. This can give rise to a quantum spin liquid ground state, in which fluctuations prevent magnetic order even at very low temperature, and in which particulary exotic magnetic excitations are predicted [13,145,146]. This is, in fact, the motivation for much of the current interest in $RuCl_3$.

4. Summary and Conclusions

The binary transition-metal halides MX_2 and MX_3 reviewed here have simple layered crystal structures containing triangular and honeycomb transition metal nets, yet they display a wide variety of interesting crystallographic and magnetic behaviors. Several compounds display polymorphism, with multiple layered and non-layered structures reported. Temperature and pressure induced crystallographic phase transitions are observed in some. Dimerization of transition metal cations results in a quenching of the magnetic moment in materials like TiX_3 and $MoCl_3$. All of the materials which maintain a local magnetic moment are observed to order magnetically, although the magnetic order in $TiCl_2$ is not definitively confirmed. This compound and the vanadium dihalides clearly show evidence of geometrical frustration of strong antiferromagnetic interactions on their triangular lattices, with ordering temperatures an order of magnitude smaller than their Weiss temperatures. Effects of a different kind of frustration, due to competing anisotropic exchange interactions, is observed in $RuCl_3$, making it a promising candidate for the realization of a Kitaev spin liquid. It appears that the in-plane magnetic interactions are at least partly ferromagnetic in most of the other magnetic MX_2 and MX_3 compounds, and field induced phase transitions that may arise from competing magnetic interactions and multiple low energy magnetic configurations are observed in several of cases. Several dihalides adopt helimagnetic structures and develop electric polarization at their magnetic ordering temperature, providing an interesting class of multiferroic materials. Finally, interest is growing in producing monolayer magnetic materials from several of these compounds, in particular the chromium trihalides, which will enable exciting advances in functional van der Waals heterostructures. Particularly interesting for this application is the wide variety of in-plane magnetic structures that occur in MX_2 and MX_3 compounds. Although several of these materials have been studied for many decades, it is likely that layered, binary, transition-metal halides will continue to provide a fruitful playground for solid state chemists, physicists, and materials scientists seeking to further our understanding of low dimensional magnetism and to develop new functional materials.

Acknowledgments: This work is supported by the US Department of Energy, Office of Science, Basic Energy Sciences, Materials Sciences and Engineering Division.

Conflicts of Interest: The author declares no conflict of interest.

References

1. De Jongh, L.J. *Magnetic Properties of Layered Transition Metal Compounds*; Kluwer Academic Press: Dordrecht, The Netherlands, 1990.
2. Kadowaki, H.; Ubukoshi, K.; Hirakawa, K.; Martinez, J.L.; Shirane, G. Experimental Study of New Type Phase Transition in Triangular Lattice Antiferromagnet VCl_2. *J. Phys. Soc. Jpn.* **1987**, *56*, 4027–4039.
3. Ramirez, A.P. Strongly Geometrically Frustrated Magnets. *Annu. Rev. Mater. Sci.* **1994**, *24*, 453–480.
4. Collins, M.F.; Petrenko, O.A. Triangular antiferromagnets. *Can. J. Phys.* **1997**, *75*, 605–655.
5. Tokunaga, Y.; Okuyama, D.; Kurumaji, T.; Arima, T.; Nakao, H.; Murakami, Y.; Taguchi, Y.; Tokura, Y. Multiferroicity in $NiBr_2$ with long-wavelength cycloidal spin structure on a triangular lattice. *Phys. Rev. B* **2011**, *84*, 060406(R).
6. Kurumaji, T.; Seki, S.; Ishiwata, S.; Murakawa, H.; Tokunaga, Y.; Kaneko, Y.; Tokura, Y. Magnetic-Field Induced Competition of Two Multiferroic Orders in a Triangular-Lattice Helimagnet MnI_2. *Phys. Rev. Lett.* **2011**, *106*, 167206.

7. Wu, X.; Cai, Y.; Xie, Q.; Weng, H.; Fan, H.; Hu, J. Magnetic ordering and multiferroicity in MnI_2. *Phys. Rev. B* **2012**, *86*, 134413.
8. Kurumaji, T.; Seki, S.; Ishiwata, S.; Murakawa, H.; Kaneko, Y.; Tokura, Y. Magnetoelectric responses induced by domain rearrangement and spin structural change in triangular-lattice helimagnets NiI_2 and CoI_2. *Phys. Rev. B* **2013**, *87*, 014429.
9. Plumb, K.W.; Clancy, J.P.; Sandilands, L.J.; Shankar, V.V.; Hu, Y.F.; Burch, K.S.; Kee, H.Y.; Kim, Y.J. α-$RuCl_3$: A spin-orbit assisted Mott insulator on a honeycomb lattice. *Phys. Rev. B* **2014**, *90*, 041112.
10. Kim, H.; Shankar V.; Catuneanu, A.; Kee, H. Kitaev magnetism in honeycomb $RuCl_3$ with intermediate spin-orbit coupling. *Phys. Rev. B* **2015**, *91*, 241110(R).
11. Sears, J.A.; Songvilay, M.; Plumb, K.W.; Clancy, J.P.; Qiu, Y.; Zhao, Y.; Parshall, D.; Kim, Y.J. Magnetic order in α-$RuCl_3$: A honeycomb-lattice quantum magnet with strong spin-orbit coupling. *Phys. Rev. B* **2015**, *91*, 144420.
12. Johnson, R.D.; Williams, S.C.; Haghighirad, A.A.; Singleton, J.; Zapf, V.; Manuel, P.; Mazin, I.I.; Li, Y.; Jeschke, H.O.; Valenti, R.; et al. Monoclinic crystal structure of α-$RuCl_3$ and the zigzag antiferromagnetic ground state. *Phys. Rev. B* **2015**, *92*, 235119.
13. Banerjee, A.; Bridges, C.A.; Yan, J.Q.; Aczel, A.A.; Li, L.; Stone, M.B.; Granroth, G.E.; Lumsden, M.D.; Yiu, Y.; Knolle, J.; et al. Proximate Kitaev quantum spin liquid behaviour in a honeycomb magnet. *Nat. Mater.* **2016**, *15*, 733.
14. Geim, A.K.; Geigorieva, I.V. Van der Waals heterostructures. *Nature* **2013**, *499*, 419–425.
15. Wang, H.; Eyert, V.; Schwingenschlögl, U. Electronic structure and magnetic ordering of the semiconducting chromium trihalides $CrCl_3$, $CrBr_3$, and CrI_3. *J. Phys. Condens. Matter* **2011**, *23*, 116003.
16. McGuire, M.A.; Dixit, H.; Cooper, V.R.; Sales, B.C. Coupling of Crystal Structure and Magnetism in the Layered, Ferromagnetic Insulator CrI_3. *Chem. Mater.* **2015**, *27*, 612–620.
17. Zhang, W.B.; Qu, Q.; Zhu, P.; Lam, C.H. Robust intrinsic ferromagnetism and half semiconductivity in stable two-dimensional single-layer chromium trihalides. *J. Mater. Chem. C* **2015**, *3*, 12457–12468.
18. Liu, J.; Sun, Q.; Kawazoe, Y.; Jena, P. Exfoliating biocompatible ferromagnetic Cr-trihalide monolayers. *Phys. Chem. Chem. Phys.* **2016**, *18*, 8777–8784.
19. Wang, H.; Fan, F.; Zhu, S.; Wu, H. Doping enhanced ferromagnetism and induced half-metallicity in CrI_3 monolayer. *EPL* **2016**, *114*, 47001.
20. Zhong, D.; Seyler, K.L.; Linpeng, X.; Cheng, R.; Sivadas, N.; Schmidgall, B.H.E.; Taniguchi, T.; Watanabe, K.; McGuire, M.A.; Yao, W.; et al. Van der Waals Engineering of Ferromagnetic Semiconductor Heterostructures for Spin and Valleytronics. *arXiv* **2017**, arXiv:1704.00841.
21. Huang, B.; Clark, G.; Navarro-Moratalla, E.; Klein, D.R.; Cheng, R.; Seyler, K.L.; Zhong, D.; Schmidgall, E.; McGuire, M.A.; Cobden, D.H.; et al. Layer-dependent Ferromagnetism in a van der Waals Crystal down to the Monolayer Limit. *arXiv* **2017**, arXiv:1703.05892.
22. Lebègue, S.; Björkman, T.; Klintenberg, M.; Nieminen, R.M.; Eriksson, O. Two-Dimensional Materials from Data Filtering and Ab Initio Calculations. *Phys. Rev. X* **2013**, *3*, 031002.
23. Ajayan, P.; Kim, P.; Banerjee, K. Two-dimensional van der Waals materials. *Phys. Today* **2016**, *69*, 38.
24. Park, J. Opportunities and challenges of 2D magnetic van der Waals materials: Magnetic graphene? *J. Phys. Condens. Matter* **2016**, *28*, 301001.
25. MacDonald, A.H.; Tsoi, M. Antiferromagnetic metal spintronics. *Philos. Trans. R. Soc. A* **2011**, *369*, 3098–3114.
26. Gomonay, E.V.; Loktev, V.M. Spintronics of antiferromagnetic systems. *Low Temp. Phys.* **2014**, *40*, 17.
27. Jungwirth, T.; Marti, X.; Wadley, P.; Wunderlich, J. Antiferromagnetic spintronics. *Nat. Nanotechnol.* **2016**, *11*, 231.
28. Klemm, W.; Krose, E. Die Kristallstrukturen von $ScCl_3$, $TiCl_3$ und VCl_3. *Z. Anorg. Chem.* **1947**, *253*, 218–225.
29. Natta, G.; Corradini, P.; Allegra, G. The different crystalline modifications of $TiCl_3$, a catalyst component for the polymerization of α-olefins. I: α-, β-, γ-$TiCl_3$. II: δ-$TiCl_3$. *J. Polym. Sci.* **1961**, *51*, 399–410.
30. Von Schnering, H.G.; Wöhrle, H.; Schäfer, H. Die Kristallstruktur der Verbindung Nb_3Cl_8. *Naturwissenschaften* **1961**, *48*, 159.
31. Sheckelton, J.P.; Plumb, K.W.; Trump, B.A.; Broholm, C.L.; McQueen, T.M. Rearrangement of van der Waals stacking and formation of a singlet state at T = 90 K in a cluster magnet. *Inorg. Chem. Front.* **2017**, *4*, 481–490.

32. Jiang, J.; Liang, Q.; Meng, R.; Yang, Q.; Tan, C.; Sun, X.; Chen, X. Exploration of new ferromagnetic, semiconducting and biocompatible Nb_3X_8 (X = Cl, Br or I) monolayers with considerable visible and infrared light absorption. *Nanoscale* **2017**, *9*, 2992–3001.
33. Brehzer, B. Röntgenographische Untersuchungen an $ZnCl_2$. *Naturwissenschaften* **1959**, *46*, 106b.
34. Yamaguchi, S. Determining the crystal structure of hygroscopic substances by electron diffraction: $ZnBr_2$. *Sci. Pap. Inst. Phys. Chem. Res. (Jpn.)* **1942**, *39*, 291.
35. Yamaguchi, S. Determining the crystal structure of hygroscopic substances by electron diffraction (continued): ZnI_2. *Sci. Pap. Inst. Phys. Chem. Res. (Jpn.)* **1942**, *39*, 357.
36. Pauling, L. On the crystal structure of the chlorides of certain bivalent elements. *Proc. Natl. Acad. Sci. USA* **1929**, *15*, 709–712.
37. Mitchell, R.S. Single crystal x-ray study of structural polytypism in cadmium bromide. *Z. Kristallogr.* **1962**, *117*, 309.
38. Bozorth, R.M. The crystal structure of cadmium iodide. *J. Am. Chem. Soc.* **1922**, *44*, 2232–2236.
39. Bijvoet, J.M.; Claassen, A.; Karssen, A. The Crystal Structure of Red Mercuric Iodide. *Proc. K. Ned. Akad. Wet.* **1926**, *29*, 529–546.
40. Schneider, M.; Kuske, P.; Lutz, H.D. Novel High-Temperature Polymorphs of $MgBr_2$ and $MnBr_2$—Limits of Powder Diffraction for Structure Determination. *Acta Crystallogr. B* **1992**, *48*, 761–763.
41. Kuindersma, S.R.; Sanchez, J.P.; Haas, C. Magnetic and Structural Investigations on NiI_2 and CoI_2. *Phys. B Condens. Matter* **1981**, *111*, 231–248.
42. Narath, A.; Schirber, J.E. Effect of Hydrostatic Pressure on the Metamagnetic Transitions in $FeCl_2{\cdot}2H_2O$, $CoCl_2{\cdot}2H_2O$, $FeCl_2$, and $FeBr_2$. *J. Appl. Phys.* **1966**, *37*, 1124.
43. Rozenberg, G.K.; Pasternak, M.P.; Gorodetsky, P.; Xu, W.M.; Dubrovinsky, L.S.; LeBihan, T.; Taylor, R.D. Pressure-induced structural, electronic, and magnetic phase transitions in $FeCl_2$ studied by x-ray diffraction and resistivity measurements. *Phys. Rev. B* **2009**, *79*, 214105.
44. Baenziger, N.C.; Rundle, R.E. The structure of $TiCl_2$. *Acta Crystallogr.* **1948**, *1*, 274.
45. Ehrlich, P.; Gutsche, W.; Seifert, H.J. Darstellung und Kristallstruktur von Titandibromid. *Z. Anorg. Allg. Chem.* **1961**, *312*, 80–86.
46. Klemm, W.; Grimm, L. Zur Kenntnis der Dihalogenide des Titans und Vanadins. *Z. Anorg. Allg. Chem.* **1942**, *249*, 198–208.
47. Villadsen, J. Note on the Crystal Structure of Vanadium Dichloride. *Acta Chem. Scand.* **1959**, *13*, 2146.
48. Kuindersma, S.R.; Hass, C.; Sanchez, J.P.; Al, R. Magnetic structures and properties of VI_2. *Solid State Commun.* **1979**, *30*, 403.
49. Tornero, J.D.; Fayos, J. Single crystal structure refinement of $MnCl_2$. *Z. Kristallogr.* **1990**, *192*, 147.
50. Wollan, E.O.; Koehler, W.C.; Wilkinson, M.K. Neutron Diffraction Study of the Magnetic Properties of $MnBr_2$. *Phys. Rev.* **1958**, *110*, 638.
51. Ferrari, A.; Giorgi, F. La struttura cristallina degli ioduri anidri dei metalli bivalenti. I. Ioduri di cobalto, di ferro e di manganese. *Atti Accad. Naz. Lincei Cl. Sci. Fis. Mat. Nat. Rend.* **1929**, *10*, 522.
52. Vettier, C.; Yellon, W.B. The structure of $FeCl_2$ at high pressures. *J. Phys. Chem. Solids* **1975**, *36*, 401–405.
53. Haberecht, J.; Borrmann, H.; Kniep, R. Refinement of the crystal structure of iron dibromide, $FeBr_2$. *Z. Kristallogr. New Cryst. Struct.* **2001**, *216*, 510.
54. Gelard, J.; Fert, A.R.; Mériel, P.; Allain, Y. Magnetic structure of FeI_2 by neutron diffraction experiments. *Solid State Commun.* **1974**, *14*, 187–189.
55. Grimme, H.; Santos, J.A. The Structure and Colour of Anhydrous Cobalt Chloride, $CoCl_2$, at Room and very Low Temperatures. *Z. Kristallogr.* **1934**, *88*, 136–141.
56. Ferrari, A.; Giorgi, F. La struttura cristallina dei bromuri di metalli bivalenti. *Atti Accad. Naz. Lincei Cl. Sci. Fis. Mat. Nat. Rend.* **1929**, *9*, 1134.
57. Ferrari, A.; Braibanti, A.; Bigliardi, G. Refinement of the crystal structure of $NiCl_2$ and of unit-cell parameters of some anhydrous chlorides of divalent metals. *Acta Crystallogr.* **1963**, *16*, 846–847.
58. Nasser, J.A.; Kiat, J.M.; Gabilly, R. X-ray investigation of magnetostriction in $NiBr_2$. *Solid State Commun.* **1992**, *82*, 49–54.
59. Ketalaar, J.A.A. Die Kristallstruktur des Nickelbromids und -jodids. *Z. Kristallogr.* **1934**, *88*, 26.

60. Cisar, A.; Corbett, J.D.; Daake, R.L. The zirconium dichloride phase region. Synthesis, structure, and photoelectron spectral studies of 3R-$ZrCl_2$, 6T-$Zr_{1.05}Cl_2$, and related phases. *Inorg. Chem.* **1979**, *18*, 836–843.
61. Guthrie, D.H.; Corbett, J.D. Synthesis and Structure of an Infinite-Chain Form of ZrI_2 (α). *J. Solid State Chem.* **1981**, *37*, 256–263.
62. Corbett, J.D.; Guthrie, D.H. A second infinite-chain form of zirconium diiodide (β) and its coherent intergrowth with α-zirconium diiodide. *Inorg. Chem.* **1982**, *21*, 1747.
63. Imoto, H.; Corbett, J.D.; Cisar, A. Synthesis by hydrogen-driven disproportionation reactions. Synthesis and structure of the hexazirconium dodecahalide clusters Zr_6Cl_{12} and Zr_6Br_{12} and the double salt $Zr_6Cl_{12} \cdot M_2ZrCl_6$ (M= Na, K, Cs). *Inorg. Chem.* **1981**, *20*, 145.
64. Men'kov, A.A.; Komissarova, L.N. An X-ray diffraction study of scandium bromide. *Russ. J. Inorg. Chem.* **1964**, *9*, 952.
65. Men'kov, A.A.; Komissarova, L.N. X-ray diffraction study of scandium iodide. *Russ. J. Inorg. Chem.* **1964**, *9*, 425.
66. Templeton, D.H.; Darter, G.F. The crystal structure of Yttrium Trichloride and similar compounds. *J. Phys. Chem.* **1954**, *58*, 940–944.
67. Brown, D.; Fletcher, S.; Holah, D.G. The Preparation and Crystallographic Properties of Certain Lanthanide and Actinide Tribromides and Tribromide Hexahydrates. *J. Chem. Soc. A* **1968**, 1889–1894.
68. Jongen, L.; Meyer, G. Yttrium triiodide, YI_3. *Acta Crystallogr. E* **2005**, *61*, i151–i152.
69. Poineau, F.; Johnstone, E.V.; Czerwinski, K.R.; Sattelberger, A.P. Recent Advances in Technetium Halide Chemistry. *Acc. Chem. Res.* **2013**, *47*, 624–632.
70. Troyanov, S.I.; Snigireva, E.M.; Rybakov, V.B. An X-ray structural investigation of the phase transition in α-$TiCl_3$. *Russ. J. Inorg. Chem.* **1991**, *36*, 634.
71. Troyanov, S.I.; Rybakov, V.B.; Ionov, V.M. The synthesis and crystal structures of $TiBr_4$, $TiBr_3$, and $Ti(AlBr_4)_2$. *Russ. J. Inorg. Chem.* **1990**, *35*, 494.
72. McCarley, R.E.; Roddy, J.W.; Berry, K.O. Transport reactions of some vanadium(III) halides. Mixed halide formation. *Inorg. Chem.* **1964**, *3*, 50.
73. Morosin, B.; Narath, A. X-Ray Diffraction and Nuclear Quadrupole Resonance Studies of Chromium Trichloride. *J. Chem. Phys.* **1964**, *40*, 1958–1967.
74. Handy, L.L.; Gregory, N.W. Structural Properties of Chromium(III) Iodide and Some Chromiurn(III) Mixed Halides. *J. Am. Chem. Soc.* **1952**, *74*, 891–893.
75. Hashimoto, S.; Forster, K.; Moss, S.C. Structure refinement of an $FeCl_3$ crystal using a thin plate sample. *J. Appl. Crystallogr.* **1989**, *22*, 173–180.
76. Troyanov, S. Crystal Structure of $FeCl_3$ Polytypes. *Russ. J. Inorg. Chem.* **1993**, *38*, 1821.
77. Armbrüster, M.; Ludwig, T.; Rotter, H.W.; Thiele, G.; Oppermann, H. About Irontribromide: Equilibrium Studies, Crystal Structure, and Spectroscopic Characterization. *Z. Anorg. Allg. Chem.* **2000**, *626*, 187.
78. Schäfer, H.; von Schnering, H.G.; Tillack, J.V.; Kuhnen, F.; Wörle, H.; Baumann, H. Neue Untersuchungen über die Chloride des Molybdäns. *Z. Anorg. Allg. Chem.* **1967**, *353*, 281–310.
79. Poineau, F.; Johnstone, E.V.; Weck, P.F.; Forster, P.M.; Kim, E.; Czerwinski, K.R.; Sattelberger, A.P. β-technetium trichloride: Formation, structure, and first-principles calculations. *Inorg. Chem.* **2012**, *51*, 4915.
80. Cao, H.B.; Banerjee, A.; Yan, J.; Bridges, C.A.; Lumsden, M.D.; Mandrus, D.G.; Tennant, D.A.; Chakoumakos, B.C.; Nagler, S.E. Low-temperature crystal and magnetic structure of α-$RuCl_3$. *Phys. Rev. B* **2016**, *93*, 134423.
81. Fletcher, J.M.; Gardner, W.E.; Fox, A.C.; Topping, G. X-Ray, Infrared, and Magnetic Studies of α- and β-Ruthenium Trichloride. *J. Chem. Soc. A* **1967**, 1038–1045.
82. Stroganov, E.V.; Ovchinnikov, K.V. Crystal structure of ruthenium trichloride. *Vestn. Leningr. Univ. Ser. 4* **1957**, *22*, 152.
83. Bärnighausen, H.; Handa, B.K. Die Kristallstruktur von Rhodium(III)-Chlorid. *J. Less-Common Met.* **1964**, *6*, 226–231.
84. Brodersen, K.; Thiele, G.; Recke, I. Strukturuntersuchungen an Rhodiumhalogeniden. *J. Less-Common Met.* **1968**, *14*, 151–152.
85. Brodersen, K.; Moers, F.; von Schnering, H.G. Zur Struktur des Iridium(III)- und des Ruthenium(III)-chlorids. *Naturwissenschaften* **1965**, *52*, 205–206.

86. Brodersen, K.; Thiele, G.; Ohnsorge, H.; Recke, I.; Moers, F. Die Struktur des $IrBr_3$ und über die Ursachen der Fehlordnungserscheinungen bei den in Schichtenstrukturen kristallisierenden Edelmetalltrihalogeniden. *J. Less-Common Met.* **1968**, *15*, 347–354.
87. Ogawa, S. Magnetic Transition in $TiCl_3$. *J. Phys. Soc. Jpn.* **1960**, *15*, 1901.
88. Troyanov, S.I.; Snigireva, E.M.; Pirarevskii, A.P.; Yanovskii, A.I.; Struchkov, Y.T. Crystal Structure of α-$TiBr_3$ Low-Temperature Modification. *Russ. J. Inorg. Chem.* **1994**, *39*, 360.
89. Troyanov, S.I.; Snigireva, E.M. Crystal Structures of Transition-Metal Halides $TiCl_4$, α-$TiCl_3$, WCl_4, and TiI_2. *Russ. J. Inorg. Chem.* **2000**, *45*, 580.
90. Park, S.Y.; Do, S.H.; Choi, K.Y.; Jang, D.; Jang, T.H.; Schefer, J.; Wu, C.M.; Gardner, J.S.; Park, J.M.S.; Park, J.H.; Ji, S. Emergence of the Isotropic Kitaev Honeycomb Lattice with Two-dimensional Ising Universality in α-$RuCl_3$. *arXiv* **2016**, arXiv:1609.05690.
91. Babel, D.; Deigner, P. Die Kristallstruktur von β-Iridium(III)-Chlorid. *Z. Anorg. Allg. Chem.* **1965**, *339*, 57–66.
92. Kim, H.S.; Kee, H.Y. Crystal structure and magnetism in α-$RuCl_3$: An ab initio study. *Phys. Rev. B* **2016**, *93*, 155143.
93. Zhou, Y.; Lu, H.; Zu, X.; Gao, F. Evidencing the existence of exciting half-metallicity in two-dimensional $TiCl_3$ and VCl_3 sheets. *Sci. Rep.* **2016**, *6*, 19407.
94. Khomskii, D.I. *Transition Metal Compounds*; Cambridge University Press: Cambridge, UK, 2014.
95. Niel, M.; Cros, C.; Le Flem, G.; Pouchard, M.; Hagenmuller, P. Magnetic behaviour of vanadium +II in one- and two-dimensional systems. *Phys. B Condens. Matter* **1977**, *702*, 86–88.
96. Lewis, J.; Machin, D.J.; Newnham, I.E.; Nyholm, R.S. The Magnetic Properties of Some Halides of Titanium and Zirconium. *J. Chem. Soc.* **1962**, p. 2036–2041.
97. Starr, C.; Bitter, R.; Kaufmann, A.R. The Magnetic Properties of the Iron Group Anhydrous Chlorides at Low Temperatures. *Phys. Rev.* **1940**, *58*, 977.
98. Hirakawa, K.; Kadowaki, H.; Ubukoshi, K. Study of Frustration Effects in Two-Dimensional Triangular Lattice Antiferromagnets−Neutron Powder Diffraction Study of VX_2, $X \equiv$ Cl, Br and I. *J. Phys. Soc. Jpn.* **1983**, *52*, 1814–1824.
99. Kadowaki, H.; Ubukoshi, K.; Hirakawa, K. Neutron Scattering Study of the Triangular-Lattice Antiferromagnet VBr_2. *J. Phys. Soc. Jpn.* **1985**, *54*, 363–373.
100. Abdul Wasey, A.H.M.; Karmakar, D.; Das, G.P. Manifestation of long-range ordered state in layered VX_2 (X = Cl, Br, I) systems. *J. Phys. Condens. Matter* **2013**, *25*, 476001.
101. Murray, R.B. Specific Heat of Single-Crystal $MnCl_2$ in Applied Magnetic Fields. *Phys. Rev.* **1962**, *128*, 1570.
102. Wilkinson, M.K.; Cable, J.W.; Wollan, E.O.; Koehler, W.C. *Oak Ridge National Laboratory Report*; Oak Ridge National Laboratory: Oak Ridge, TN, USA, 1958, Volume ORNL-2430, p. 65.
103. Wiesler, D.G.; Suzuki, M.; Suzuki, I.S.; Rosov, N. Determination of Anomalous Superexchange in $MnCl_2$ and Its Graphite Intercalation Compound. *Phys. Rev. Lett.* **1995**, *75*, 942.
104. Sato, T.; Kadowaki, H.; Iio, K. Successive phase transitions in the hexagonal-layered Heisenberg antiferromagnets MnX_2 (X = Br, I). *Phys. B Condens. Matter* **1995**, *224*, 213–214.
105. Cable, J.W.; Wilkinson, M.K.; Wollan, E.O.; Koehler, W.C. Neutron Diffraction Investigation of the Magnetic Order in MnI_2. *Phys. Rev.* **1962**, *125*, 1860–1864.
106. Katsumata, K.; Aruga Katori, H.; Kimura, S.; Narumi, Y.; Hagiwara, M.; Kindo, K. Phase transition of a triangular lattice Ising antiferromagnet FeI_2. *Phys. Rev. B* **2010**, *82*, 104402.
107. Bertrand, Y.; Fert, A.R.; Gélard, J. Susceptibilité magnétique des halogénures ferreux $FeCl_2$, $FeBr_2$, FeI_2. *J. Phys.* **1974**, *35*, 385–391.
108. Wilkinson, M.K.; Cable, J.W.; Wollan, E.O.; Koehler, W.C. Neutron Diffraction Investigations of the Magnetic Ordering in $FeBr_2$, $CoBr_2$, $FeCl_2$, and $CoCl_2$. *Phys. Rev.* **1959**, *113*, 497.
109. Fert, A.R.; Carrara, P.; Lanusse, M.C.; Mischler, G.; Redoules, J.P. Transition de phase metamagnetique du bromure ferreux. *J. Phys. Chem. Solids* **1973**, *34*, 223–230.
110. Xu, W.M.; Pasternak, M.P. Magnetism in $FeCl_2$ at High Pressures. *Hyperfine Interact.* **2002**, *175*, 144–145.
111. Pasternak, M.P.; Xu, W.M.; Rozenberg, G.K.; Taylor, R.D.; Hearne, G.R.; Sterer, E. Pressure-induced magnetic and electronic transitions in the layered Mott insulator FeI_2. *Phys. Rev. B* **2001**, *65*, 035106.
112. Jacobs, I.S.; Lawrence, P.E. Metarnagnetic Phase Transitions and Hysteresis in $FeCl_2$. *Phys. Rev.* **1967**, *164*, 866.

113. Fert, A.R.; Gelard, J.; Carrara, P. Phase Transitions of FeI_2 in High Magnetic Field Parallel to the Spin Direction, Static Field up to 150 kOe, Pulsed Field up to 250 kOe. *Solid State Commun.* **1973**, *13*, 1219–1223.
114. Lines, M.E. Magnetic Properties of $CoCl_2$ and $NiCl_2$. *Phys. Rev.* **1963**, *131*, 546.
115. Binek, C.; Kleemann, W. Domainlike antiferromagnetic correlations of paramagnetic $FeCl_2$: A field-induced Griffiths phase? *Phys. Rev. Lett.* **1994**, *72*, 1287.
116. Binek, C.; Bertrand, D.; Regnault, L.P.; Kleemann, W. Magnetic neutron-scattering investigation of the field-induced Griffiths phase in $FeCl_2$. *Phys. Rev. B* **1996**, *54*, 9015.
117. Katsumata, K.; Aruga Katori, H.; Shapiro, S.M.; Shirane, G. Neutron-scattering studies of a phase transition in the metamagnet $FeBr_2$ under external magnetic fields. *Phys. Rev. B* **1997**, *55*, 11466.
118. Chisholm, R.C.; Stout, J.W. Heat capacity and entropy of $CoCl_2$ and $MnCl_2$ from 11 degrees to 300 degrees K−thermal anomaly associated with antiferromagnetic ordering in $CoCl_2$. *J. Chem. Phys.* **1962**, *36*, 972–979.
119. Yoshizawa, H.; Ubukoshi, K.; Hirakawa, K. Neutron Scattering Investigation of the Magnetic Excitations in $CoBr_2$. *J. Phys. Soc. Jpn.* **1980**, *48*, 42–49.
120. Mekata, M.; Kuriyama, H.; Ajiro, Y.; Mitsuda, S.; Yoshizawa, H. First-order magnetic transition in CoI_2. *J. Magn. Magn. Mater.* **1992**, *859*, 104–107.
121. Friedt, J.M.; Sanchez, J.P.; Shenoy, G.K. Electronic and magnetic properties of metal diiodides MI_2 (M = V, Cr, Mn, Fe, Co, Ni, Cd) from I-129 Mössbauer spectroscopy. *J. Chem. Phys.* **1976**, *65*, 5093–5102.
122. Busey, R.H.; Giauque, W.F. The Heat Capacity of Anhydrous $NiCl_2$ from 15 to 300 K. The Antiferromagnetic Anomaly near 52 K. Entropy and Free Energy. *J. Am. Chem. Soc.* **1952**, *74*, 4443–4446.
123. Adam, A.; Billery, D.; Terrier, C.; Mainard, R.; Regnault, L.P.; Rossat-Mignod, J.; Mériel, P. Neutron diffraction study of the commensurate and incommensurate magnetic structures of $NiBr_2$. *Solid State Commun.* **1980**, *35*, 1–5.
124. De Gunzbourg, J.; Papassimacopoulos, S.; Miedan-Gros, A.; Allain, Y. Étude Expérimentale du Chlorure de Nickel par Rotation Faraday et Mesures Magnétiques en Champ Statique et Pulsé. *J. Phys. Colloq.* **1971**, *32*, C1–C125.
125. Pollard, R.J.; McCann, V.H.; Ward, J.B. Electronic and magnetic properties of ^{57}Fe in $NiCl_2$, $NiBr_2$, NiI_2 and CoI_2 from Mössbauer spectroscopy. *J. Phys. C Solid State Phys.* **1982**, *15*, 6807.
126. Day, P.; Dinsdale, A.; Krausz, E.R.; Robbins, D.J. Optical and neutron diffraction study of the magnetic phase diagram of $NiBr_2$. *J. Phys. C Solid State Phys.* **1976**, *9*, 2481.
127. Day, P.; Ziebeck, K.R.A. Incommensurate spin structure in the low-temperature magnetic phase of $NiBr_2$. *J. Phys. C Solid State Phys.* **1980**, *13*, L523.
128. Billery, D.; Terrier, C.; Ciret, N.; Kleinclauss, J. Neutron diffraction study and specific heat of antiferromagnetic NiI_2. *Phys. Lett. A* **1977**, *61*, 138.
129. He, J.; Ma, S.; Lyu, P.; Nachtigall, P. Unusual Dirac half-metallicity with intrinsic ferromagnetism in vanadium trihalide monolayers. *J. Mater. Chem. C* **2016**, *4*, 2518–2526.
130. Tsubokawa, I. On the Magnetic Properties of a $CrBr_3$ Single Crystal. *J. Phys. Soc. Jpn.* **1960**, *15*, 1664–1668.
131. Hansen, W.N. Some Magnetic Properties of the Chromium (III) Halides at 4.2 K. *J. Appl. Phys.* **1959**, *30*, S304–S305.
132. Dillon, J.F., Jr.; Olson, C.E. Magnetization, Resonance, and Optical Properties of the Ferromagnet CrI_3. *J. Appl. Phys.* **1965**, *36*, 1259–1260.
133. Cable, J.W.; Wilkinson, M.K.; Wollan, E.O. Neutron Diffraction Investigation of Antiferromagnetism in $CrCl_3$. *J. Phys. Chem. Solids* **1961**, *19*, 29–34.
134. Kuhlow, B. Magnetic Ordering in $CrCl_3$ at the Phase Transition. *Phys. Stat. Sol. A* **1982**, *72*, 161–168.
135. Cable, J.W.; Wilkinson, M.K.; Wollan, E.O.; Koehler, W.C. Neutron-Diffraction Study of Antiferromagnetic $FeCl_3$. *Phys. Rev.* **1962**, *127*, 714.
136. Jones, E.R., Jr.; Morton, O.B.; Cathey, L.; Auel, T.; Amma, E.L. Low-Temperature Magnetic Susceptibility of $FeCl_3$. *J. Chem. Phys.* **1969**, *50*, 4755–4757.
137. Johnson, P.B.; Friedberg, S.A.; Rayne, J.A. Field-induced magnetic phase transitions in $FeCl_3$. *J. Appl. Phys.* **1981**, *52*, 1932–1934.
138. Stampfel, J.P.; Oosterhuis, W.T.; Window, B.; Barros, F. Mössbauer-Effect Measurements in Antiferromagnetic $FeCl_3$. *Phys. Rev. B* **1973**, *8*, 4371.
139. Oosterhuis, W.T.; Window, B.; Spartalian, K. Sublattice magnetization in $FeBr_3$ below the critical region. *Phys. Rev. B* **1975**, *10*, 4616.

140. Kim, B.J.; Jin, H.; Moon, S.J.; Kim, J.Y.; Park, B.G.; Leem, C.S.; Yu, J.; Noh, T.W.; Kim, C.; Oh, S.J.; et al. Novel J_{eff} = 1/2 Mott State Induced by Relativistic Spin-Orbit Coupling in Sr_2IrO_4. *Phys. Rev. Lett.* **2008**, *101*, 076402.
141. Fletcher, J.M.; Gardner, W.E.; Hooper, E.W.; Hyde, K.R.; Moore, F.H.; Woodhead, J.L. Anhydrous Ruthenium Chlorides. *Nature* **1963**, *199*, 1089–1090.
142. Kobayashi, Y.; Okada, T.; Asai, K.; Katada, M.; Sano, H.; Ambe, F. Mössbauer Spectroscopy and Magnetization Studies of α- and β-$RuCl_3$. *Inorg. Chem.* **1992**, *31*, 4570–4574.
143. Majumder, M.; Schmidt, M.; Rosner, H.; Tsirlin, A.A.; Yasuoka, H.; Baenitz, M. Anisotropic Ru^{3+} $4d_5$ magnetism in the α-$RuCl_3$ honeycomb system: Susceptibility, specific heat, and zero-field NMR. *Phys. Rev. B* **2015**, *91*, 180401.
144. Kitaev, A. Anyons in an exactly solved model and beyond. *Ann. Phys.* **2006**, *321*, 2–111.
145. Baskaran, G.; Mandal, S.; Shankar, R. Exact Results for Spin Dynamics and Fractionalization in the Kitaev Model. *Phys. Rev. Lett.* **2007**, *98*, 247201.
146. Knolle, J.; Kovrizhin, D.L.; Chalker, J.T.; Moessner, R. Dynamics of a Two-Dimensional Quantum Spin Liquid: Signatures of Emergent Majorana Fermions and Fluxes. *Phys. Rev. Lett.* **2014**, *112*, 207203.